THESIS FOR THE DEGREE OF LICENTIATE OF ENGINEERING

Carbon capture using industrial side-streams as absorbents

EMMANOUELA LEVENTAKI

Department of Chemistry and Chemical Engineering

CHALMERS UNIVERSITY OF TECHNOLOGY

Gothenburg, Sweden 2023

Carbon capture using industrial side-streams as absorbents

EMMANOUELA LEVENTAKI

© EMMANOUELA LEVENTAKI, 2023.

Technical report no 2023:18

Department of Chemistry and Chemical Engineering
Chalmers University of Technology
SE-412 96 Gothenburg
Sweden
Telephone + 46 (0)31-772 1000

Cover: Illustration by Emmanouela Leventaki

Printed by Chalmers Digitaltryck
Gothenburg, Sweden 2023

Carbon capture using industrial side-streams as absorbents

EMMANOUELA LEVENTAKI

Department of Chemistry and Chemical Engineering

Chalmers University of Technology

Abstract

Recent predictions about climate change underscore the need to take drastic measures toward more sustainable and environmentally friendly practices. Reducing the emission of greenhouse gases and improving waste management are pertinent to this goal. A resourceful approach for carbon capture is to use industrial alkaline side-streams as absorbents of CO_2 which could offer environmental and economic benefits.

Alkaline side-streams are present in many industries, such as paper and pulp manufacturing, iron and steel production and others. Their alkalinity comes from their content in metal oxides or hydroxides. These compounds can react with CO_2 towards the formation of carbonates. Carbonation occurs naturally between atmospheric CO_2 and earth minerals, at very slow rates. To accelerate this process water can be used as a medium to dissolve the metal oxides and facilitate the interaction between dissolved compounds coming from the industrial side-streams and CO_2 from flue gas.

There are many pathways for exploration in this topic, such as the potential of different side-streams to capture CO_2 based on their availability and carbon capture capacity, the prospects of utilization for the carbonated products, etc. This work focuses on answering some of these questions for five industrial side-streams. Firstly, an experimental setup was established using aqueous solutions of NaOH as a CO_2 absorbent. Following that two side-streams of the paper and pulp industry and three of the steelmaking process were examined. The paper and pulp side-streams were black liquor and green liquor dregs. Black liquor has a high content of NaOH and it exhibited an absorption capacity of 30.8 g of CO_2 / L. Green liquor dregs are a solid material rich in CaO and MgO. They were mixed with water at different concentrations and the maximum capture capacity obtained was 18 g of CO_2 / L of mixture. Steelmaking slags contain CaO along with other metal complexes. The best-performing steel slag mixture had a maximum capacity of 38.7 g of CO_2 / L of mixture.

This work paves the way to study the absorption capacity of more side-streams and offers a solid background upon which the carbonation process could be optimized and tailored to each type of side-stream for the purpose of industrial application.

Keywords: Carbon capture, Aqueous carbonation, Alkaline side-streams

Acknowledgements

This work is funded by the Swedish Energy Agency and samples used for the experiments were provided by SCA and Höganäs. I am thankful to my colleagues at the Decrease project for their passion and ideas and for always striving to advance our research. The Chalmers Materials Analysis Laboratory (CMAL) is acknowledged for the SEM images and XRD diffractograms.

I would like to express my gratitude to my supervisor Diana Bernin and co-supervisor Francisco Baena-Moreno for offering me the opportunity to work on this project and for always being by my side throughout this time. Their support, understanding and trust have greatly helped me in reaching this milestone. I aspire to have the love for science, limitless ideas and kindness of Diana and it has been my honor being the first PhD student of someone as intelligent and driven as Fran.

I am also very thankful for everyone in my division. Phuoc's coffee, his eagerness to help with anything and take care of people have made the division a great place to work. Michael has been a good friend and his patience when I am chasing him in the corridors asking for help with the smallest things should not go unrecognized. Joanna was the perfect office mate, offering me many moments of fun. I am glad I got to spend these two years working close to her. The division is full of amazing people, and I am lucky for getting the chance to be around them.

A special thank you is also due to anyone and anything that makes my life fuller. The friends I made throughout the years, the travels and adventures I have experienced, good music and good books are the best and most important parts of life.

Finally, I would like to thank my family, who have always believed in me. I would not have gotten this far without their care and encouragement.

List of publications

The thesis is based on the following appended papers:

Paper I: Effluents and residues from industrial sites for CO_2 capture: a review

Francisco M. Baena Moreno, **Emmanouela Leventaki**, Alexander Riddell, Joanna Wojtasz Mucha, Diana Bernin

Environmental Chemistry Letters, Volume 21, Issue 1, 2023, 319-337.

Paper II: In-Line Monitoring of CO_2 Capture with NaOH in a Customized 3D-Printed Reactor without Forced Mixing

Emmanouela Leventaki, Francisco M. Baena Moreno, Gaetano Sardina, Henrik Ström, Ebrahim Ghahramani, Shirin Naserifar, Phuoc Hoang Ho, Aleksandra M. Kozlowski, Diana Bernin

Sustainability, Volume 14, 2022, 10795.

Paper III: Potential of organic carbonates production for efficient CO_2 capture, transport and storage: Reaction performance with NaOH–ethanol mixtures

Francisco M. Baena Moreno, **Emmanouela Leventaki**, Phuoc Hoang Ho, Abdul Raouf Tajik, Danica Brzic, Gaetano Sardina, Henrik Strom, Diana Bernin

Heliyon, Volume 9, Issue 3, 2023, e14140, ISSN 2405-8440.

Paper IV: Experimental evaluation of black liquor carbonation for CO_2 capture

Emmanouela Leventaki, Francisco M. Baena Moreno, Joanna Wojtasz Mucha, Niclas Sjöstedt, Abdul Raouf Tajik, Gaetano Sardina, Henrik Ström, Diana Bernin

Journal of CO2 Utilization, Volume 72, 2023, 102516, ISSN 2212-9820.

Publications not included in this thesis:

Paper V: **Solid–Liquid Phase Transitions of Triglycerides in Griebenschmalz, Smalec, and Fedt Studied Using 13C Solid-State NMR with Dynamics-Based Spectral Filtering**

Diana Bernin, **Emmanouela Leventaki**, Daniel Topgaard

Applied Magnetic Resonance, 1-11, 2023.

Contribution report

Paper I (Co-author): I wrote sections of the manuscript. I reviewed and edited the article along with Francisco M. Baena Moreno, Alexander Riddell, Joanna Wojtasz Mucha, Diana Bernin.

Paper II (First author): I designed the reactor. I planned and performed all experiments together with Francisco M. Baena Moreno. Phuoc Hoang Ho conducted the XRD analysis. Gaetano Sardina performed CFD simulations. I wrote the manuscript. I reviewed and edited the article along with the co-authors.

Paper III (Co-author): I designed the reactor. I assisted with the experiments. I reviewed and edited the article along with the co-authors.

Paper IV (First author): I planned and performed all experiments. I conducted the XRD analysis. I took SEM images together with Francisco M. Baena Moreno. Diana Bernin did the NMR analysis. Abdul Raouf Tajik performed the CFD simulations. I wrote the manuscript. I reviewed and edited the article along with the co-authors.

Table of Contents

1. Introduction 1
   1.1. CO_2 and climate change 1
   1.2. Carbon capture routes and technologies 1
   1.3. Alkaline industrial by-products for carbon capture 3
2. Background 6
   2.1. Carbon capture with NaOH 6
   2.2. Paper and pulp side-streams 7
      2.2.1. Black liquor 8
      2.2.2. Green liquor dregs 9
      2.2.3. Steelmaking slag 9
3. Materials and Methods 10
   3.1. Materials 10
   3.2. Methods 11
      3.2.1. Reactor design 11
      3.2.2. Evolution of the carbonation reactions 14
      3.2.3. CO_2 absorption rate and capacity 15
      3.2.4. Post-carbonation characterization 16
      3.2.5. CFD simulations 17
4. Results 18
   4.1. CFD evaluation of the mixing inside the two types of reactors 18
   4.2. Monitoring the evolution of carbonation using in-line FTIR and pH 20
   4.3. Absorption capacity 26
   4.4. Physicochemical characterization of the carbonates 31
5. Conclusions 39
6. Future perspectives 40
7. References 41

1. Introduction

1.1. CO_2 and climate change

Greenhouse gases (GHGs) surround the surface of the Earth and maintain its temperature at habitable levels by absorbing the radiation emitted by the planet. Despite their valuable role, the increased release of these gases into the atmosphere due to human activities has led to an abnormal rise in the average temperature, which results in a chain of adverse environmental changes and threatens our way of life [1]. The main GHGs are water vapor, CO_2, CH_4, N_2O and fluorinated gases. The highest emitted gas from human activities is CO_2, contributing to over 79% of the total GHG emissions [2]. To reduce the release of human-related GHGs several intergovernmental policies have been put in place. According to the most recent report of IPCC some changes towards sustainability have been implemented, but more rapid reduction of GHGs emissions is required [3]. To this end, different types of renewable energy sources and GHG removal processes should work synergistically to reach global goals [4]. Carbon capture specifically targets the emission of CO_2 and its subsequent storage (CCS) or utilization (CCU) [5]. This process is intended to be implemented temporarily, during the transition away from fossil fuels. By combining renewable energy with accelerated CO_2 sinks it might be feasible to create negative carbon emissions and restore the natural carbon cycle.

1.2. Carbon capture routes and technologies

There are four main routes of carbon capture depending on the type of gas stream from which the CO_2 is collected: pre-combustion, post-combustion, oxy-fuel combustion, and direct air capture (DAC) [6]. In the pre-combustion route, fossil fuel is gasified to produce syngas, which is a mixture of H_2 and CO. CO reacts with water towards the formation of H_2 and CO_2. The concentrated CO_2 (15-60%) in the flue gas can then be captured. Post-combustion capture refers to the CO_2 generated from fuel combustion with air. Since air contains a low amount of oxygen the concentration of CO_2 in the flue gas is proportionally low (3-20%). In oxy-fuel combustion, the fuel is burned in an atmosphere of almost pure oxygen, producing the highest concentration of CO_2. Finally, in DAC the gas is collected directly from the atmosphere, where its concentration is on average 420 ppm.

Over the last years, there has been constant development of carbon capture technologies targeting the separation of the gas from the aforementioned types of sources. The main categories of these technologies, along with some examples are shown in Figure 1. Chemical absorption possesses benefits in terms of efficiency and selectivity that have earned its recognition as the most suitable option for the

separation of CO_2 from post-combustion flue gas [7]. The main families of chemical absorbents are amines, caustic and carbonate solutions, ammonia and ionic liquids [8]. Of these, monoethanolamine (MEA) and other amines are the most extensively studied and used absorbents [9]. CO_2 absorption technologies, primarily with the use of amines, are utilized commercially at industrial processes for the purification of gas streams. However, they are still not widely applied in power plants, specifically for the purpose of carbon capture and storage. That is because the cost of CO_2 separation processes is more significant compared to the carbon emission penalties that companies are required to pay [10]. Furthermore, the use of amines entails severe challenges, such as the volatility, degradation and highly corrosive nature of the compounds, as well as their energy-intensive regeneration, which could be surpassed by choosing more easily manageable absorbents [11]–[13].

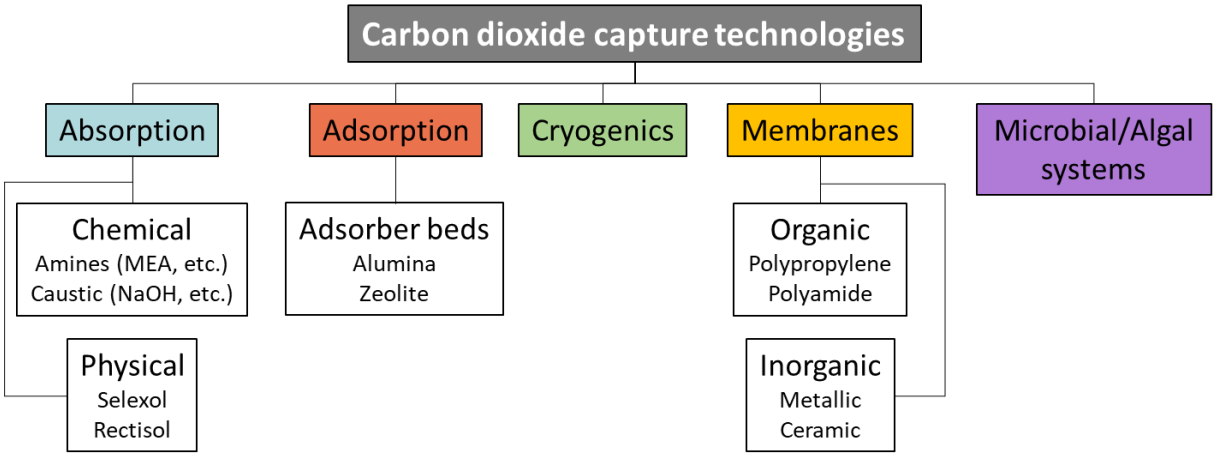

Figure 1. Carbon capture technologies. Modified from [6], [10], [14].

Alkaline solutions, such as NaOH, KOH and $Ca(OH)_2$ have lower performance compared to amines, but they are nevertheless considered to be efficient absorbents. CO_2 is absorbed in alkaline solutions via aqueous carbonation. The chemical reactions between such solutions and CO_2 are quite straightforward and have been thoroughly researched [15]–[18], while industrial application has also received its fair share of attention [19]–[21]. The advantage of alkaline materials over other absorbents is their abundance and availability. Metal oxides and hydroxides exist in a wide range of industrial processes and as a consequence, there are several alkaline residual streams that can readily react with CO_2 [22]. These industrial effluents, which are typically either used as rest products or landfilled, can instead be utilized in carbon capture, thus reducing the need for new raw materials. According to the literature, the amount of available alkaline residues that have carbon capture potential is currently too low in comparison to the rate of CO_2 emissions. But future trends of material consumption for human activities indicate an increase in industrial side-streams which can serve as significant carbon sinks [23]. This inevitable rise of residues emphasizes the need to properly utilize them and carbon capture offers this possibility. However, there is a

variety of alkaline residues with different chemical compositions, mechanical properties, availability, etc. Thus, it is crucial to evaluate the capacity of these materials to capture CO_2 and identify challenges and opportunities that might be presented along the way.

1.3. Alkaline industrial side-streams for carbon capture

Paper I offers a review of alkaline side-streams with potential in carbon capture via carbonation and documents scientific efforts found in literature towards this purpose. The materials covered in this work were steelmaking slags, municipal solid waste incinerator ashes, combustion fly ashes, black liquor, paper mill waste, mining waste, cement waste, construction and demolition waste, waste from the organic industry, and flue gas desulfurization gypsum waste. These streams typically contain inorganic chemicals such as Ca, Na, K, Mg, and other metals like Fe or Al. Often, disposal of such materials in landfill can lead to the leaching of harmful compounds. By reacting them with CO_2 their pH can drop to more neutral levels and the carbonated products could potentially find use as green alternatives to conventional building materials in constructions, or as fillers for abandoned mines [24]–[27]. Thus, the CO_2 can remain stored in the form of stable metal carbonates presumably for many years.

As discussed in **Paper I**, the carbonation of industrial side-streams can be either direct or indirect. Direct carbonation can occur either in gas-solid or gas-aqueous systems, where the gas comes in contact with the solid waste either in dry conditions or mixed with water in a one-step process. In indirect carbonation, the waste is first treated for the extraction of metal ions and then the gas reacts with the leached metal ions in a separate step. Depending on the type of process the final product can be either a heterogeneous material rich in carbonates (direct carbonation) or pure metal carbonates (indirect carbonation) [22]. Pure metal carbonates are valuable products with many applications, but the multiple-step process for leaching the metal ions requires more energy than a one-step process. The products that result from direct carbonation are mixtures of various chemical compounds. Thus post-carbonation analysis is needed to evaluate the properties of these products and determine applications where they could find use. Table 1 presents the side-streams studied in this review along with their carbon capture capacity reported in the the literature, possible utilization pathways for the carbonated products and the annual global production of each stream. References for the carbon capture data reported in Table 1 can be found in **Paper I**. Literature suggests that direct aqueous carbonation can yield higher absorption capacities in steelmaking slag [28] and municipal solid waste incinerator ashes [29], [30].

Table 1. Comparison of wastes from different industries in regard to their absorption capacity reported in literature and their annual production.

Industry	Waste	Capture capacity range (kg / ton of waste)	Potential end life of final product	Worldwide production (Mmt)	Global production ref.
Iron & Steel	Steelmaking slag	Gas-solid: 10–50 Aqueous: 200–300 Indirect: 100–250	Reuse in concrete, Asphaltic paving	190–280	[31]
Energy	Municipal solid waste incinerator ashes	Gas-solid: 20–120 Aqueous: 200–260	Reuse in concrete, Disposal for CO_2 storage	2000–57000*	Estimated
	Combustion fly ash	Gas-solid: 2–20	Reuse in concrete	300–400	[32]
Paper and Pulp	Black liquor	Not evaluated	Recovery of lignin for biochemicals, Recovery of CO_2 and storage	Approximately 1300	[33]
	Paper mill waste	218–460	Reuse in concrete, CO_2 storage	Data not available	
Mining	Mining waste	Approximately 130	Pacify hazardous waste, CO_2 storage	Approximately 100000	[34]
Cement	Cement waste	Gas-solid: 81–800** Indirect cannot be evaluated	Reuse in concrete, Soil stabilization	217–352*	Estimated
Construction	Construction and demolition waste	Gas-solid: 45–417	Reuse in concrete	2400–3600	[35]
Organic chemicals	Organic waste	4.0–17.7	Production of organic carbonates, CO_2 storage	Data not available	-
Other	Flue gas desulfurization gypsum waste	530–800***	Reuse in concrete	Approximately 30	[36]

*Value estimated from available data of raw materials.

**Experiments carried out under humid conditions in contrast with the other wastes here reviewed. High values correspond to high humidity ratios.

***CO_2 captured via a different methodology in a two-stages process.

Carbonation can also take place in alcohol solutions, but it has not been researched extensively [37]–[40]. Alcohols, such as ethanol, isopropanol and others can be found in side-streams of industries dealing with organic chemicals, such as pharmaceuticals, polyvinyl alcohol fibers, paints and coatings, etc. [41], [42]. These alcohols could be used in combination with metal hydroxides to react with CO_2 towards the production of carbonates, which are insoluble in alcohol and form a dispersion system. This

concept was explored in **Paper III** with the use of NaOH-ethanol solutions as absorbents. The solid carbonate particles can be easily separated from the alcohol medium and the CO_2 can be recovered by the addition of water or acid. The generated CO_2 could then be transported to geological sequestration sites for storage.

While there are a lot of studies evaluating the potential of various wastes in carbon capture using different methods of carbonation, in **Paper I** the authors identified industrial side-streams that have not been explored yet. There is no or very little research on the absorption of CO_2 with the use of black liquor, green liquor dregs and alcohol waste, to name a few. This thesis is an effort to cover some gaps in this field. Initially, aqueous solutions of pure NaOH were used as absorbents to establish an experimental methodology and provide the foundation for future experiments (**Paper II**). Following that, various industrial side-streams were investigated for their carbonation potential. **Paper IV** is a study conducted on the carbonation of black liquor, a by-product of the paper and pulp industry with high alkalinity owing to its content in NaOH. One more paper and pulp residue, namely green liquor dregs, and three by-products of the steelmaking process were obtained from Swedish industrial partners and preliminary exploration of the carbonation of these materials will also be presented here. The focus of all the studies was threefold: to follow the carbonation reactions between each absorbent and the CO_2 in the gas stream, to estimate the absorption capacity of each solvent and to study the products formed after the reactions using various analytical techniques. The project is conducted in collaboration with experts in Computational Fluid Dynamics (CFD) and Life Cycle Assessment (LCA). The CFD studies aim to optimize the reactor design for future scale-up and the LCA work will evaluate the feasibility of using different side-streams in carbon capture.

2. Background

In this section the absorbent systems that have been studied experimentally will be introduced. The systems are aqueous NaOH, two side-streams of the paper and pulp industry and three side-streams of the steelmaking industry.

2.1. Carbon capture with NaOH

NaOH is highly soluble in water and relatively soluble in ethanol [44]. When a gaseous stream containing CO_2 is bubbled through aqueous solutions of NaOH the absorption occurs in a series of steps [45]–[47].

The mass transfer of CO_2 is one of the limiting steps, during which CO_2 from the bulk of the gaseous stream is transferred to the interphase between the bubbles and the liquid. From there the following reactions take place.

$$CO_{2(g)} \leftrightarrow CO_{2(aq)} \tag{1}$$

$$NaOH_{(s)} \leftrightarrow NaOH_{(aq)} \leftrightarrow Na^+ + OH^- \tag{2}$$

$$CO_{2(aq)} + OH^- \leftrightarrow HCO_3^- \tag{3}$$

$$HCO_3^- + OH^- \leftrightarrow CO_3^{2-} + H_2O \tag{4}$$

Reaction (4) is considered instantaneous and occurs at high pH. At the beginning of the process, when the concentration of hydroxides is very high and the equilibrium of equation (4) is driven strongly towards the right side, then the presence of the intermediate HCO_3^- is insignificant and the absorption of CO_2 can be described with equation (5) [47].

$$CO_{2(aq)} + 2OH^- \leftrightarrow CO_3^{2-} + H_2O \tag{5}$$

As CO_2 keeps flowing, the hydroxide is depleted and the equilibrium of equation (4) is gradually shifted towards the left, while at the same time newly introduced CO_2 follows equation (3). Consequently, at the pH range between 12 and 8, $\boldsymbol{HCO_3^-}$ is forming as a result of both the absorption of CO_2 and from the already present CO_3^{2-} via equation (4) [48]. At pH below 8 the equations (6) and (7) take place [45].

$$CO_{2(aq)} + H_2O \leftrightarrow H_2CO_{3(aq)} \tag{6}$$

$$HCO_3^- \leftrightarrow H_2CO_{3(aq)} + H^+ \tag{7}$$

In contrast to CO_3^{2-} and HCO_3^-, H_2CO_3 is a lot less soluble in water and therefore below the pH of 8 the absorption of CO_2 is negligible [49]–[51].

2.2. Paper and pulp side-streams

Figure 2 shows a simplified overview of the typical operation of a paper and pulp industry. The lignocellulosic feedstock is fed in a digester where it is treated with a process called Kraft pulping to break down the wood and separate cellulose from the lignins and hemicelluloses [52]. The chemical treatment is done with white liquor, a solution of NaOH and Na_2S. The process has been optimized over the years to have maximum recovery of chemicals and be energy efficient in every step, yet there are still effluents such as black liquor, green liquor dregs, fly ash, slacker grits and lime mud which could be managed better [53]. Currently, black liquor is burned for energy, while other wastes are commonly either incinerated or landfilled. Since most of these streams are alkaline, containing sodium, calcium and other metals, carbonation could be a potential way to valorize them.

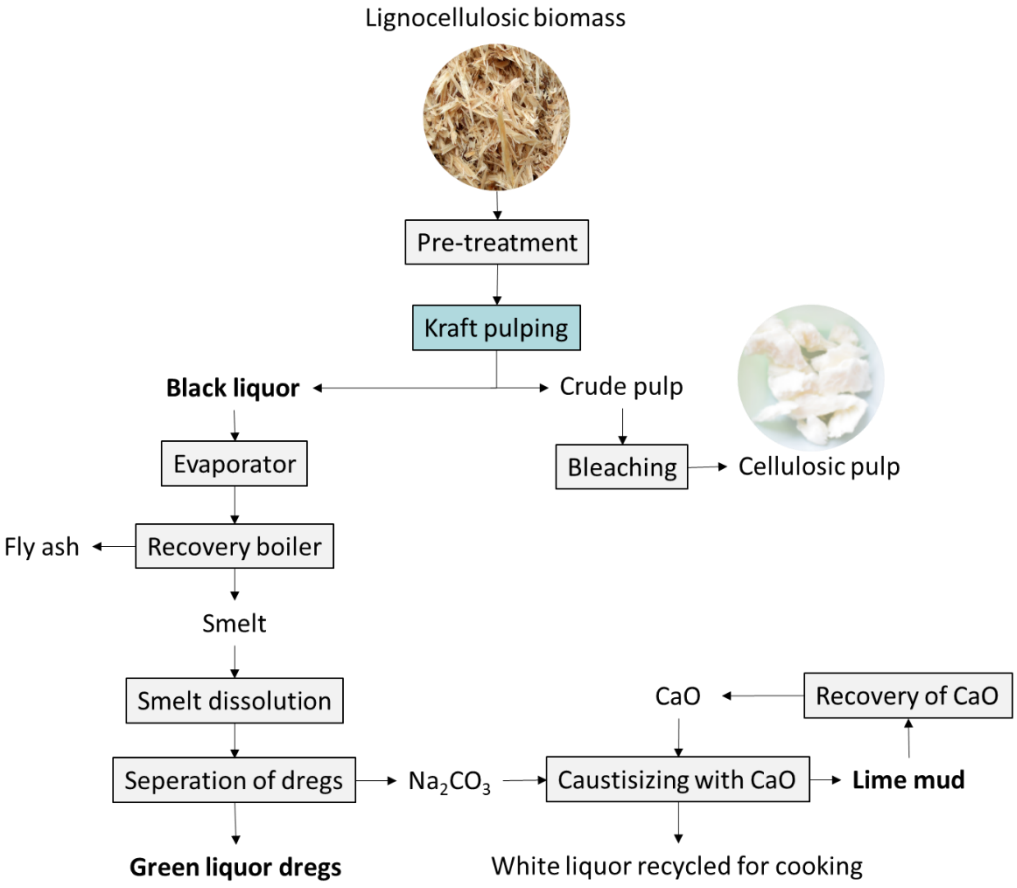

Figure 2. Simplified scheme of a typical industrial paper and pulp process, modified from [54]–[56].

2.2.1. Black liquor

Black liquor is the by-product of pulping [57], [58]. Industrially the main process used for pulping is Kraft cooking, which is very efficient for wood, but recently, non-woody biomass has also received attention as a valuable feedstock for cellulose production [56]. Agricultural residues such as oat husks, wheat straws, rice straws and more, are abundant, they are produced at very rapid rates and have high annual yields of cellulose [59], [60]. The treatment of these materials can be done with soda pulping, which employs the use of an aqueous NaOH solution with concentrations between 2 and 17% w/v [61]. From this process the main product is cellulose and the spent solution is black liquor. The composition of non-woody black liquor depends greatly on the feedstock. Generally, it contains 0-36% of lignin, in dry weight, as well as hemicelluloses, soap, saccharides and other organic compounds. It can also contain 0.4–16% silica (% dry weight) and other inorganic molecules, which are mainly NaOH and some Na_2CO_3 from the cooking [62]–[64].

Industrially, black liquor passes through evaporators to reduce its water content and is then sent to a recovery boiler for energy generation. Subsequently, the inorganic matter left in the recovery boiler is processed to recover pure NaOH and sodium sulfide which are recycled in the cooking step. An alternative to burning black liquor is the extraction of lignin and hemicellulose from it, which have multiple applications in biorefineries or other processes [65]. The most common method to extract lignin from black liquor is by lowering the pH [66], [67]. Lignin is soluble at high alkalinity, but it starts precipitating as the pH is reduced and it is completely insoluble at the pH of 2 [68], [69]. To this end, black liquor can be combined with flue gas to absorb CO_2 via the carbonation reactions mentioned in section 2.1. and consequently, lower the pH of the liquor to a minimum of 8 to initiate lignin precipitation. The carbonated black liquor can then be further acidified to recover gaseous CO_2 and obtain a high yield of lignin. More alternatives for the utilization of carbonated black liquor could be developed, but they have not been explored in this work. The carbonation of Kraft black liquor can be challenging owing to its content in Na_2S. As the pH drops S^{2-} turns to HS^- and at the pH of 9.5 H_2S starts to form. While the first two are soluble salts, H_2S is a highly toxic gas [70]. Thus, containment of this gas would be a matter of concern in this case. For black liquor coming from soda pulping, its use as a CO_2 absorbent can be more straightforward. Silica, which tends to be quite present in non-woody biomass, precipitates at the pH range of 8-10. Since silica can cause fouling in recovery boilers, its removal is very beneficial. However, for the purpose of carbon capture, if carbonated black liquor is sent to the recovery boiler the captured CO_2 should be recovered first, so as to not be released again during the burning process. Though bubbling CO_2 through black liquor has been studied before to lower its pH, it has never been proposed as a method for carbon capture. In our work, we investigated the absorption of CO_2 in black liquor produced from soda pulping of oat husks.

2.2.2. Green liquor dregs

As can be seen in Figure 2 the incineration of black liquor generates an inorganic smelt. Water is added to this dissolve its constituents and the dissolution, called green liquor is separated from the insoluble dregs [71]. These green liquor dregs contain CaO, MgO, Na_2O, K_2O as well as SiO_2, Al_2O_3, Fe_2O_3 and other compounds in smaller concentrations [72]. This composition makes them interesting candidates for carbon capture, but to our knowledge, this possibility has not been pursued. Instead, the majority of green liquor dregs are landfilled and only some research exists on their use to seal mine waste deposits [73], [74].

2.2.3. Steelmaking slag

Steelmaking slag is a by-product of the iron and steel industry, coming from impurities in the steelmaking furnaces [75]. These slags typically contain complexes of CaO, SiO_2 and MgO along with other metals in smaller concentrations. The utilization of steelmaking slags for carbon capture has been extensively studied both with direct and indirect methods of carbonation and with different conditions of temperature, flue gas composition, particle size, etc [28], [76]–[78]. Despite the thorough research conducted on this side-stream, large-scale implementation is still challenging, due to the variations in composition between different slags, limitations of the reactions' kinetics and high energy requirements related to the pretreatment of the slags (crushing) and other parts of the process [56]. To address these gaps, three steelmaking slags have been evaluated and preliminary experiments have been conducted to evaluate their carbon capture performance in our experimental setup. The commercial names of the slags are Petrit E, Petrit L, and Petrit T. Each one comes from a different stage in the steelmaking process: (1) electric arc furnace; (2) ladle furnace; and (3) manufacturing of direct reduced iron, respectively.

All the absorption systems above have been studied in a direct aqueous process in either a bubble column reactor or a stirred reactor. The temperature and pressure have been kept ambient, as it is believed that the aqueous phase has the potential to speed up the carbonation reactions without the need for excess energy consumption.

3. Materials and Methods

3.1. Materials

For **Paper II** standard solutions of NaOH were prepared using NaOH (VWR, 99% purity) and deionized water. Solutions were prepared at concentrations 1, 2, 3, 4, 5, 6, 7 and 8 w/w%.

In **Paper IV**, weak black liquor was obtained from soda pulping of oat husks according to steps described below [56]. Oat husks, which were used as received, were subjected to prehydrolysis to loosen the lignocellulosic structure and leach some of the hemicellulose out of the material. During this process, the raw material was immersed in a weak acid inside a 1.5 L steel autoclave which rotated at a speed of 15 rpm, at 160 °C [79]. Following that, the pretreated husks were washed thoroughly with deionized water until the pH of the washing water was neutral. Finally, the soda pulping process was used to extract the pulp from the rest of the material. The pretreated material was added again to the same autoclave together with an aqueous solution of 4 w/w% of NaOH and was rotated at the same speed at 170 °C for 2 hours [80]. After cooking, the product was filtered to separate the pulp from the weak black liquor. The dry solid weight of the liquor was determined by drying it in an oven at 50 °C. The dry solids were 8 w/w%, and this black liquor was used for all our experiments. A commercial antifoaming agent (BIM Kemi) was also added to the black liquor prior to the experiments to reduce foaming. The concentration of antifoamer used was 0.043 g/L, but the optimal amount to minimize foaming depends on the type of black liquor.

Additionally, experiments have been conducted with green liquor dregs provided by SCA and steelmaking slags (Petrit T, Petrit L and Petrit E) provided by Höganäs. All solid samples were mixed with water at concentrations of 5, 10, 15 and 20 w/v% and stirred for 24 hours preceding the carbonation experiments. Green liquor dregs were also tested at the concentration of 25 w/v%, which was avoided in the steelmaking slags, due to long carbonation times. The composition of the materials is presented in Table 2.

In all experiments, the gas flow was composed of 30% CO_2 and 70% N_2 (Linde).

Table 2. Composition of steelmaking slags and green liquor dregs as provided from the suppliers.

Composition (%)	Petrit E	Petrit L	Petrit T	Green liquor dregs*
CaO	40	48	37	25
MgO	10	13	-	12.5
SiO_2	15	11	18	1.86
Al_2O_3	6.5	9	9	0.918
FeO	25	13	-	-
Fe_2O_3	-	-	7	0.435
MnO	-	-	-	2.44
Na_2O	-	-	-	3.76
C	-	-	20	-

*The material has 45% total solids. The composition given here is expressed as a percentage of the total solids.

3.2. Methods

3.2.1. Reactor design

Two types of bubble column reactors were used in the experiments, one with forced mixing and one without. Forced mixing refers to the use of a stirrer to induce mixing between the liquid and gaseous phase. Including a stirrer in the setup requires a wider reactor diameter and it also adds an energy expense to the process. In bubble column reactors it is common to avoid forced mixing and instead ensure that the gas flow is distributed homogeneously inside the liquid so that mixing is prompted by the turbulent movement of the bubbles inside the liquid [81]. Reactors with non-forced mixing are typically long and narrow to facilitate the retention and dispersion of the gas. Both the reactors used were semi-batch systems, where the liquid is the static phase, and the gas is introduced at the bottom of the reactor.

The non-forced mixing bubble column reactor was designed using Fusion 360 and printed in a stereolithography (SLA) 3D printer (Formlabs, Form 3+). It can be divided into two parts, a narrow and long neck where the mixing is intense and a wider opening that allows the insertion of probes, such as a pH probe to track the evolution of the carbonation reactions in-line. Figure 3 shows the shape and dimensions of the reactor. It was designed to have a capacity of 60 mL of liquid and on top of this volume, some extra empty space was added to avoid liquid splashing out due to the bubbly flow. This reactor was used for **Paper II** and for the green liquor dregs and steel slags.

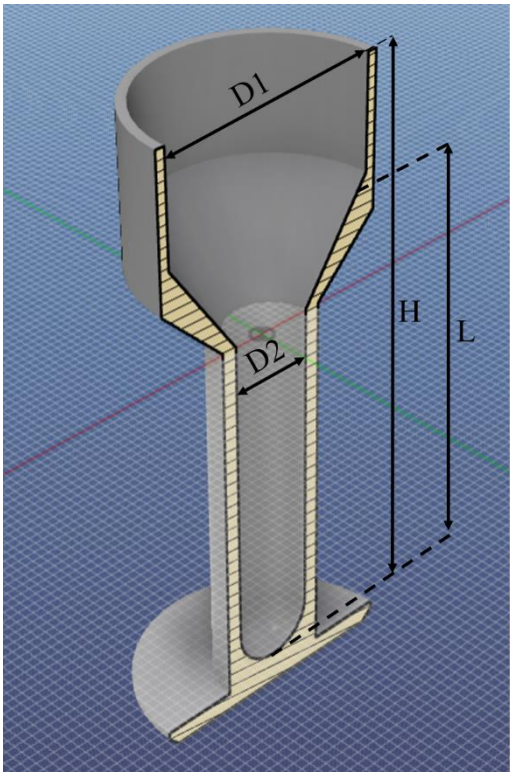

Figure 3. Reactor design and dimensions.

As the non-forced mixing reactor was successful in the carbonation of standard NaOH solutions, it was expected to be applied to the carbonation of industrial by-products as well. However black liquor proved to be a somewhat challenging liquid phase due to its tendency to foam. The foaming is caused by the presence of various fatty and rosin acid surfactants, and it can vary depending on the composition of these surfactants in the liquor [82]. Sparging gas through the black liquor caused continuous foaming which overflew the reactor, as can be seen in Figure 4. An antifoaming agent was added to change the surface tension of the liquid. This somewhat reduced the foaming, but it did not completely resolve the problem, so a mechanical stirrer (IKA®, EUROSTAR Power Control-Visc Stirrer) was also used to break the remaining foam. Therefore, for **Paper IV** the reactor was replaced with a glass beaker, wide enough to accommodate the stirrer. The volume of the liquid was this time 100 mL.

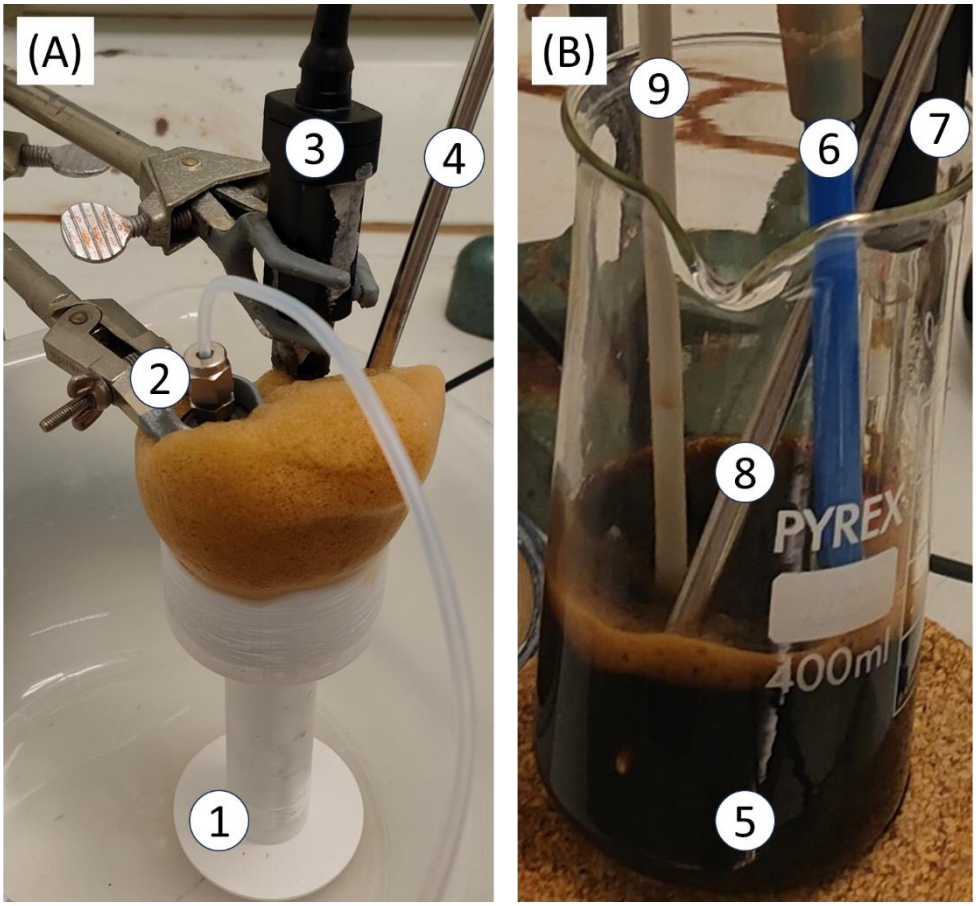

Figure 4. (A) Setup of black liquor carbonation in the 3D printed reactor: 1) Reactor, 2) Gas sparger, 3) pH probe, 4) FTIR probe. Sparging gas through the black liquor caused the formation of a very dense foam. (B) Setup of black liquor carbonation in a beaker with stirring: 5) Beaker, 6) Gas sparger, 7) pH probe, 8) FTIR probe, 9) Mechanical stirrer. The antifoamer in combination with the stirrer reduced the foaming.

In all the experiments, the gas flow was regulated with a pressure regulator and a mass flow meter. The flow rate was stable at 200 mL/m and the gas entered the reactors through a sparger (DURAN) at the bottom of the reactor. The type, orientation and positioning of the sparger is another key parameter in bubble columns. The chosen sparger has a perforated head with high porosity to induce the formation of small bubbles. In non-forced mixing reactors, the sparger head should cover a wide area so as to produce homogeneous dispersion of the bubbles throughout the liquid phase. In the 3D printed reactor this is achieved as the sparger head has a diameter of 11 mm and the reactor neck has a diameter of 22 mm. In the beaker used for the black liquor experiments, this condition was not met, but instead, the stirring enhanced the dispersion of the gas. The disadvantage of using a porous sparger is that it can easily clog in the presence of solids. Clogging is unwanted as it can build up pressure to dangerous levels and it requires a lot of maintenance [83], [84]. To minimize this phenomenon the sparger was oriented to flow gas downwards, so that any solid particles formed could collect on the bottom of the reactor, but not on the surface of the sparger head. The placement of the sparger can be seen in Figure 5. Despite this placement, in mixtures where the solid had very fine particles, such as Petrit T, the

sparger was constantly clogging. So, for the steelmaking slags the sparger was replaced by a glass tube with an opening diameter of 5 mm.

3.2.2. Evolution of the carbonation reactions

To study the carbonation reactions over time a pH probe (HQ430D, HACH) and an attenuated total reflectance Fourier transform infrared (ATR-FTIR) probe (ReactIR 702L, Mettler Toledo) were mounted inside the reactor, taking measurements in-line. Calibration of the pH meter was performed with calibration standards at pH 4, 7 and 10. The background for the FTIR probe was collected in air, spectra were taken in absorbance mode, at the wavelength range of 3000 to 640.8 cm^{-1} and with a resolution of 4 cm^{-1}. Both instruments were collecting data every 10 seconds. Figure 5A and B show the experimental setup for the two reactors. For **papers II** and **IV** the experiments were stopped when the pH reached 8, since, as mentioned above, at this pH value carbonic acid starts to form and any absorption of CO_2 beyond this point is insignificant. Green liquor dregs and steelmaking slags contain a mixture of metal oxides, the main one being CaO, and as will be seen in the results section after the pH of 8 there is still significant absorption of CO_2. More specifically, owing to the differences in composition between these materials the total equilibrium of the carbonation reactions changes and thus the pH value does not provide a clear indication of the rate of absorption. Therefore, it was decided to follow another strategy in order to identify the completion of carbonation as will be presented in the next section.

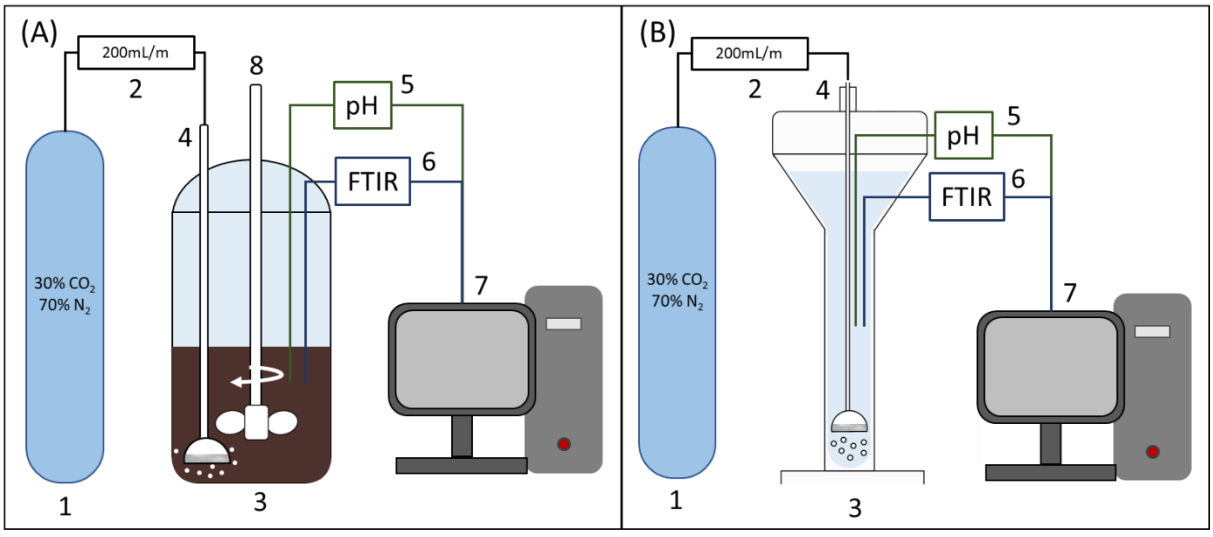

Figure 5. Experimental setup for the study of carbonation using pH and FTIR in (A) the stirred reactor and (B) the 3D printed bubble column. The numbers represent the following: 1) Gas bottle, 2) Mass flow controller, 3) Reactor, 4) Sparger, 5) pH probe, 6) FTIR probe, 7) Computer for data logging, 8) Mechanical stirrer. Both reactors were open to the atmosphere.

3.2.3. CO_2 absorption rate and capacity

To evaluate the amount of CO_2 captured in each solution an analytical balance (QUINTIX2102-1S, Sartorius), with readability of 0.01 g, was used to monitor the weight of the reactors. The increase of the weight of the reactors during the experiments was a direct result of the absorption of CO_2 into the solutions. In **Paper II** the reactor was set on the balance and the weight of the reactor was monitored continuously to obtain plots of absorption over time. The pH and FTIR probes could not be used in-line for these experiments as external forces from the wires connected to the probes were acting on the balance causing inaccuracies. For this reason, the experiments were repeated with the same conditions and the same duration as had been determined based on the pH before, but with only the sparger inside the reactor.

For **Paper IV** the duration of the experiments was also determined based on the time needed for the pH to get to 8. Then, to obtain the capture capacity of the black liquor, carbonation experiments were conducted for the same duration and the weight of the reactor was measured at the beginning and end of the process. Because of the stirrer, it was not possible to measure the weight while the experiment was going on. To ensure that the measured absorption capacity was reliable, the experiment was performed in triplicate and each time the pH was measured at the end to confirm that it was near 8.

The weight measurements can be heavily affected by weight losses in the carbonation setup. The two causes of weight losses in the system are solvent evaporation and loss of liquid that is carried away with the gas bubbles. To account for this phenomenon blank experiments were conducted with sparging only nitrogen and recording the weight decrease.

The experiments on green liquor dregs and steelmaking slags were conducted in the 3D printed reactor. The reactor was not set on the balance; instead, it was placed next to the balance and its weight was measured at regular intervals. The duration of the experiments was determined by the rate of increase of the reactor's weight. Once the balance showed the same weight two consecutive times the absorption was considered complete and the experiment was stopped. In this case, the setup was even more sensitive to weight losses than before, so a water trap was installed to eliminate the escape of liquid carried in the gas flow. The water trap consisted of a small column filled with silica beats (VWR) and placed directly at the outlet of the reactor. The setup including the water trap is displayed in Figure 6. According to the literature, silica can adsorb a very small amount of CO_2, but the silica gel used in our experiments was around 50 g, which is sufficient to collect the water, but causes an insignificant CO_2 hold-up [85], [86].

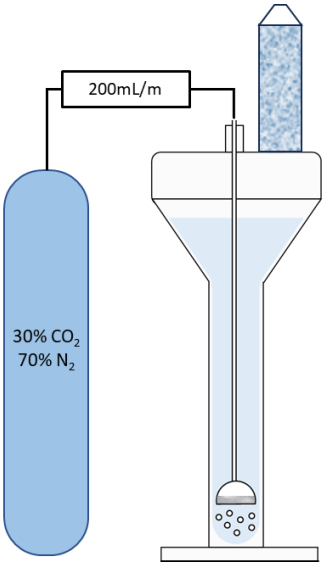

Figure 6. Experimental setup with a silica trap at the outlet of the reactor.

3.2.4. Post-carbonation characterization

The physicochemical characterization of the formed carbonates was conducted using various analytical techniques. Techniques such as x-ray diffractography (XRD) and scanning electron microscopy (SEM) require the samples to be solid. The different methods used to dry each type of solution are described next. The NaOH solutions of concentrations 5 w/w% and above exhibited solid precipitation during the carbonation reactions. The 6 w/w% carbonated solution was filtered and the separated solids were dried at ambient temperature. The carbonated black liquor was treated as follows: A part of the liquid was dried in an oven at 70 °C without further processing. Another part was filtered using filter paper number 3 (Munktell), to separate the precipitated solids from the rest of the liquid. Then both the residue and the filtrate were placed in an oven at 70 °C for two days. A sample of non-carbonated black liquor was also dried to study how carbonation affects the characteristics of the solids. The green liquor dregs and steelmaking slags were dried in an oven at 50 °C for two days.

The solid samples were ground to a fine powder and then studied with Powder XRD (D8 Discover, Bruker). The patterns were recorded for the diffraction angle (2θ) range 10 to 70° with a scan step of 0.02° per second. The diffractograms were recorded using the software DIFFRAC.EVA V5.2 and the Crystallography Open Database was used to analyze and recognize the patterns. The samples were also subjected to SEM (Phenom ProX, ThermoFisher Scientific) and the carbonated black liquor solids were also put under an optical microscope (ZEISS SteREO Discovery.V12). For the case of black liquor, liquid state ^{13}C NMR was also recorded on a Bruker Avance III HD (700 MHz Larmor frequency of ^{1}H) equipped with a QCI cryoprobe. Samples of black liquor before and after carbonation were transferred to NMR tubes, and a small amount of D_2O (Sigma, 99.8% D) was added to lock and shim the samples. A z-restored spin-echo

pulse sequence was used with 8192 scans and a repetition time of 0.1 s [87]. An exponential window function of 20 Hz was applied before the baseline correction.

3.2.5. CFD simulations

To visualize and estimate the flow field inside the two reactors and evaluate the degree of mixing between the liquid and gaseous phase, CFD simulations were performed with the use of ANSYS FLUENT (Version 2022 R2). For the non-forced mixing reactor, a 2D geometry was constructed based on the fact that if only the sparger is inside and centered then the reactor is posseces axisymmetry with respect to the z-axis (along the length of the reactor). The Euler-Euler model was employed to describe the multiphase flow and the k-ε turbulence model was used in both systems. A mixture of CO_2 and nitrogen was chosen as the gaseous phase in the non-forced mixing reactor, while air was used in the stirred reactor. The liquid was Newtonian with a viscosity of 0.0013 Pa·s, which was assumed to have similar fluid properties to both aqueous NaOH solutions and black liquor. The phases were not reactive, so as to focus only on the mixing characteristics and not add further complexity to the systems. The momentum equation included sources for drag, shear lift, wall lubrication, as well as the bubble-induced turbulence. To account for the stirring in the forced-mixing reactor the impeller was modeled in a rotating frame of reference. More detailed descriptions of the CFD models can be found in **papers II** and **IV**.

4. Results

In this section, the experimental findings that have been reported in **papers II**, **III** and **IV** will be discussed. The results are organized in four sections: CFD simulations, evolution of carbonation reactions, absorption of CO_2 and post-carbonation analysis. The CFD simulations conducted on the two types of reactors are presented first to showcase the differences in the flow patterns and examine the quality of mixing. Proceeding that, the evolution of the carbonation reactions will be introduced, based on the measurements of FTIR and pH. The NaOH aqueous solutions will be discussed first, since they provide the experimental foundation for the rest of the results and a detailed overview of the carbonation process will be given both for this system and for the black liquor. The evaluation of carbonation for the green liquor dregs and steelmaking slag samples has not yet been thoroughly studied. This section will be followed by the results on the absorption capacities of the materials, where important factors such as the rate of absorption, maximum capacity, duration of experiment and other will be discussed. Finally, the post-carbonation analysis of the materials includes results of XRD, SEM and other techniques and offers information on how the carbonation affected each material, which can provide useful knowledge for the potential utilization of the carbonated products.

4.1. CFD evaluation of the mixing inside the two types of reactors

Figure 7 shows contours of the flow obtained from the CFD simulations for the half cross-section of the reactor that was modeled. The highest gas volume fraction appears near the bottom of the reactor and it decreases towards the top, where the reactor body becomes wider, as can be seen in Figure 7A. The gas velocity, displayed in Figure 7B, is at its maximum right above the sparger head, but there seems to be motion in most parts inside the reactor. Finally, the ratio between the turbulent viscosity and molecular viscosity of the suspension is visualized in Figure 7C to evaluate the degree of mixing. It can be concluded, that solely the motion of the bubbles does not generate mixing of high intensity. This result is not unprecedented. Laboratory-scale bubble columns have been known to not be representative of industrial-size ones as the wall effects are more important, which can lead to inaccurate assessment of the mixing in the CFD simulations [88]. Other key characteristics of the 3D printed reactor that could contribute to the mixing and overall efficiency would be the ratio between height and diameter, the placement of the sparger, the use of continuous liquid flow, etc [89]. However, for this first stage of the project, optimization of the reactor was not a priority as the main focus was on the absorption capacity and evaluation of the carbonation process of different solvents. To this end, this reactor was successful in promoting interfacial chemical reactions while allowing to monitor the progression of these reactions.

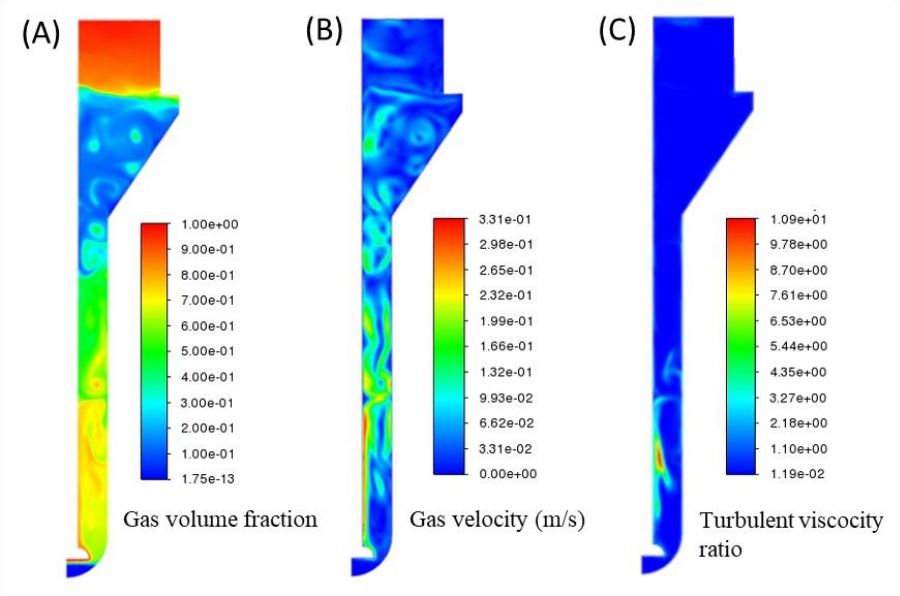

Figure 7. Contour plots of the gas volume fraction (A), gas velocity (B) and turbulent viscosity ratio (C) obtained from the CFD simulations.

In the case of the stirred reactor, the CFD simulations demonstrated that stirring at 700 rpm provides superior mixing. Figure 8A shows an iso-surface depiction of the gas velocity value of U_G = 0.3 m·s^{-1} at 0 and 700 rpm rotation of the impeller. It is evident from these contours that without stirring the gas tends to rise directly upward with minimum dispersion into the surrounding liquid. However, the introduction of stirring completely changes the profile of gas dispersion as the gas is spread around much more evenly carried by the rotation of the impeller. The gas volume fraction follows a similar pattern. In Figure 8B the iso-surface of the volume fraction α_G=0.01 is displayed and it confirms that the mixing is largely improved in the presence of stirring.

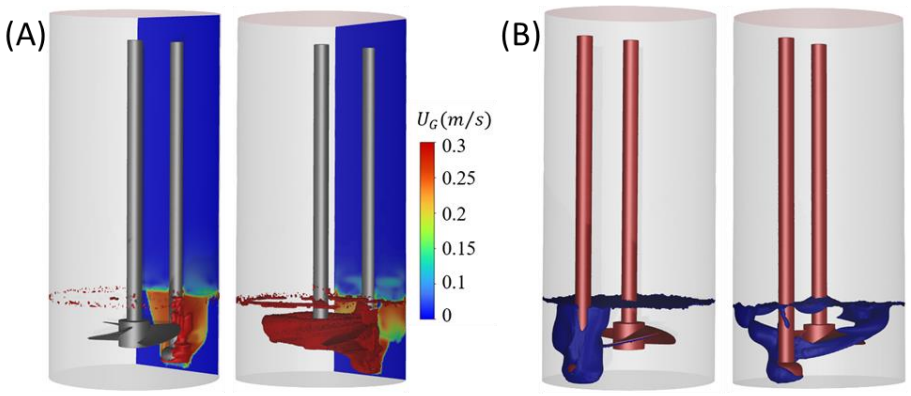

Figure 8. (A) the iso-surface of gas modulus of velocity U_G = 0.3 m·s-1 and (B) the iso-surface of gas volume fraction α_G=0.01 for Ω=0 and 700 rpm.

4.2. Monitoring the evolution of carbonation using in-line FTIR and pH

In order to validate and establish the method for monitoring the carbonation process in real-time, aqueous NaOH, a well-studied absorbent, was chosen as the reference system. The FTIR and pH data provided insight into the progression of the carbonation reactions over time. The FTIR detected the presence of CO_3^{2-} and HCO_3^- and made it possible to qualitatively track the shift in concentration between the two species based on the intensity of their respective peaks in the spectra. According to literature conducted on similar aqueous systems, CO_3^{2-} has a characteristic peak at 1395 cm^{-1}, HCO_3^- appears at 1005, 1300, 1365 and 1650 cm^{-1} and water has a very pronounced band at 1640 cm^{-1} [90], [91]. With the instrument used here, the peaks were slightly shifted to around 1380 cm^{-1} for the CO_3^{2-}, 1360, 1300 and 1008 cm^{-1}, for the HCO_3^- (the 1640 cm^{-1} band is hidden by the water band) and 1635 cm^{-1} for water. Owing to the partial overlap of the CO_3^{2-} band and the 1365 cm^{-1} band of the HCO_3^- it was not possible to extract quantitative information about the concentration of the species from the FTIR spectra. The FTIR spectra over time for different NaOH concentrations are shown in Figure 9. Initially, only the water peak is present, but as gas is sparged through the liquid the CO_3^{2-} peak becomes gradually more prominent. After some time, the shoulder of HCO_3^- at 1005 cm^{-1} appears and at the same time the band at 1395 cm^{-1} shifts towards 1365 cm^{-1} as the chemical equilibrium is shifting in favor of HCO_3^-. At low concentrations of NaOH this dynamic evolution of species is barely noticeable in the spectra, but in the solutions above 3 w/w% the spectral changes become much more significant.

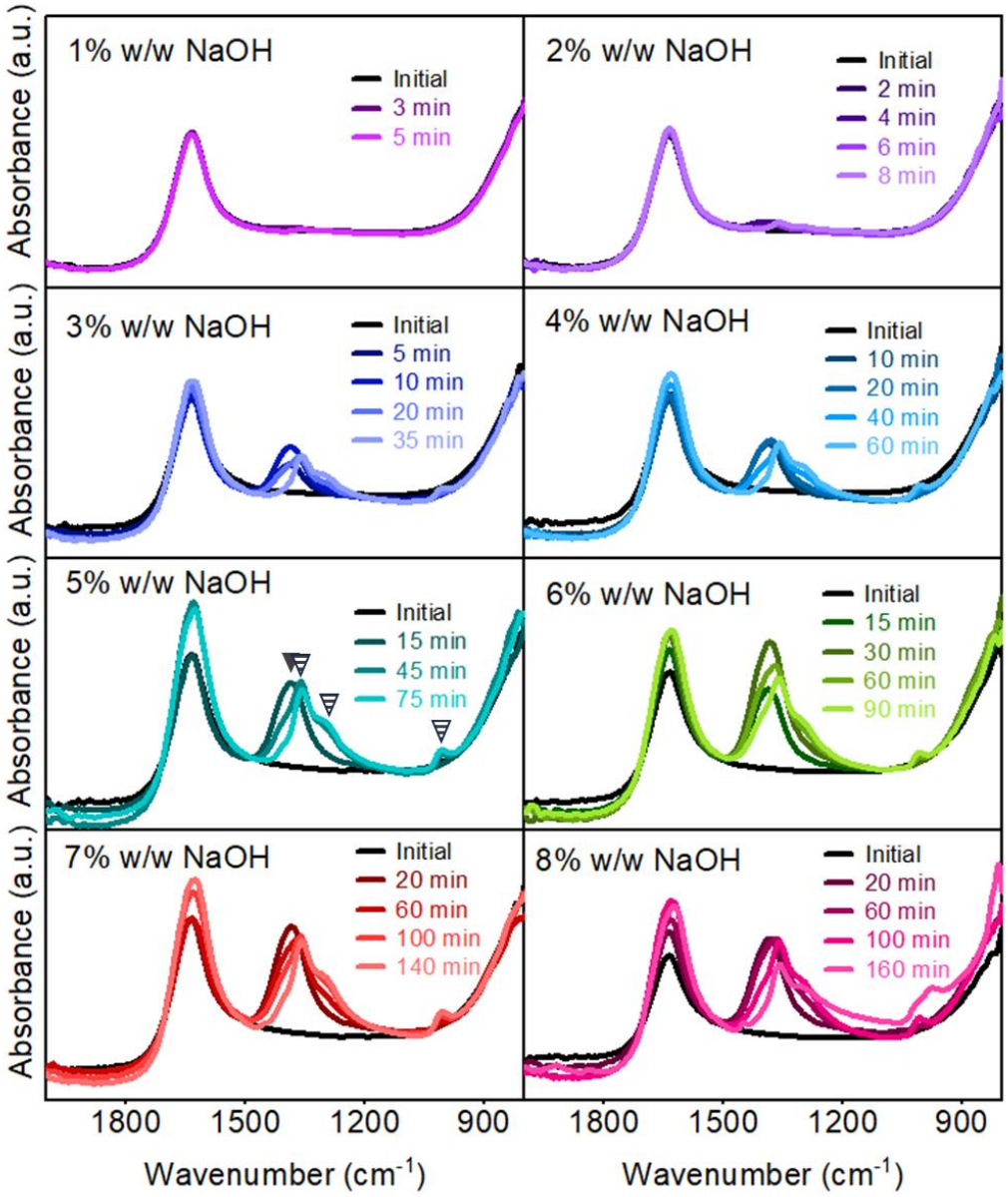

Figure 9. FTIR spectra of CO_2 absorption in the NaOH solutions over time. In the spectra of 5 w/w% NaOH the arrow with solid fill marks the peak of CO_3^{2-} at 1380 cm⁻¹ and the dashed arrows mark the peaks of HCO_3^- at 1360, 13000, and 1008 cm⁻¹.

The FTIR results along with the pH curve and the CO_2 absorption for the 4 w/w% NaOH solution were combined in Figure 10 to obtain a more holistic perspective of the progression of carbon capture in the reactor. For this purpose, the intensity of the bands at the range of 1372–1388 cm^{-1} and 1000–1016 cm^{-1} were calculated and plotted along with the pH and absorption data over time. Figure 10A shows the absorption of CO_2 in g CO_2 / L of solution. It is evident that there are three distinct regions in the plot, each one with a different rate of absorption. The highest absorption rate took place within the first 6 minutes of the experiment. The pH during this time exhibited a slow decrease from the initial value of 13.2 to 12.9, as displayed in Figure

10B. Figure 10C and D show that throughout this time CO_3^{2-} was gradually forming, while there was no sign of HCO_3^- yet. As has been discussed in chapter 2.1. high pH favors the instantaneous reaction between CO_2 and hydroxides towards the formation of CO_3^{2-}, so at this section the mass transport of the gaseous CO_2 into the liquid phase is the limiting factor. This explains the high rate of absorption.

Following this, the next absorption section lasted 18.5 minutes and during that time 19.8 g/L of CO_2 were absorbed. During this time, the pH decreased drastically. The intensity of the CO_3^{2-} absorbance reached a maximum after 12.67 minutes of the experiment, where the pH had the highest drop at the value of 11.2. The pH value at the maximum rate of decrease is known as the equivalent point, where both sides of an equation are at stoichiometric equilibrium. This equivalent point corresponds to the equilibrium of Equation (5) mentioned in 2.1. At that point, HCO_3^- started to appear (Figure 10D). This leads to the conclusion that the equivalent point marks the pH value where the depletion of hydroxides becomes significant and thus the formation of HCO_3^- according to Equation (3) and the reverse of Equation (4) is starting to become more favorable. From there on the signal intensity of the HCO_3^- peak had a steady increase at the expense of the CO_3^{2-} species.

The last section of absorption lasted 35 minutes, during which an additional 11.5 g/L of CO_2 was absorbed and the pH exhibited a very slow decline from 9.6 until 8, at which the experiment was stopped. At this pH range both the new CO_2 that flows into the reactor and the CO_3^{2-} ions in solution turn into HCO_3^-. This explains why the absorption rate is slower at this section. If this absorption system were to be implemented for large-scale CO_2 separation, the process should potentially be kept at high pH to obtain maximum and quick removal of the gas.

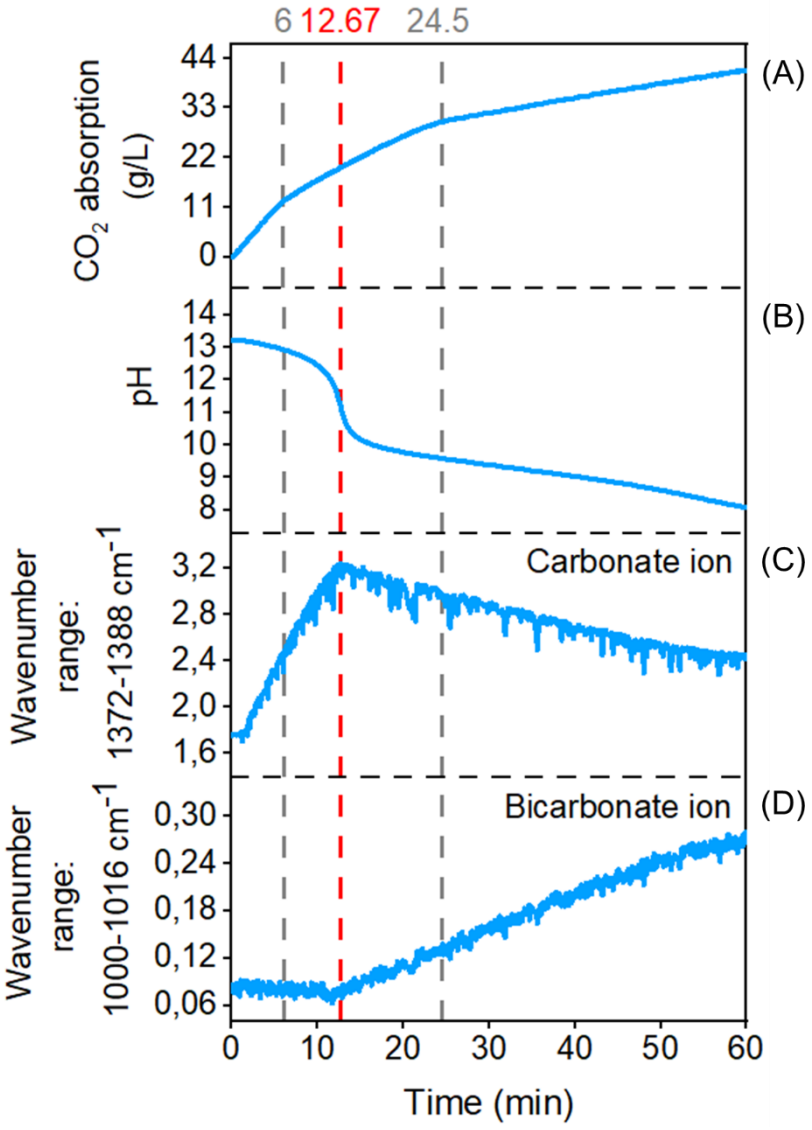

Figure 10. (A) CO_2 absorption, (B) pH, (C) Sum of the absorbance intensities of the wavenumber range 1372–1388 cm^{-1} corresponding to the CO_3^{2-} region and (D) Sum of the absorbance intensity of the wavenumber range 1000–1016 cm^{-1} corresponding to the HCO_3^- region with time for 4 w/w% NaOH.

These results are in line with findings reported in the literature, which confirms the reliability of the experimental method [92]. The black liquor followed very similar trends in the pH curve and FTIR spectra, as shown in Figure 11. The CO_3^{2-} peak was again slightly shifted to 1390 cm^{-1} and one of the HCO_3^- peaks was at 1355 cm^{-1} instead of 1360 cm^{-1}. These small variations probably stem from the difference in the chemical environment of each absorbent. The FTIR spectrum of the black liquor before the reaction shows that a small amount of CO_3^{2-} is inherently present in the material, coming from the pulping process. With the absorption of CO_2, the intensity of the CO_3^{2-} peak increased and subsequently decreased as the HCO_3^- peaks ascended. The pH curve exhibited a similar drop as the one of pure NaOH in water, with the exception that the equivalent point appeared at 11.64 instead of 11.2. This difference is hardly noteworthy, but it could reflect the fact that other molecules inside the system, such

as lignin, silica and others are also undergoing changes, e.g. precipitation, as the pH lowers. These side reactions can cause an overall alteration in the equilibrium, as portrayed in the pH measurements.

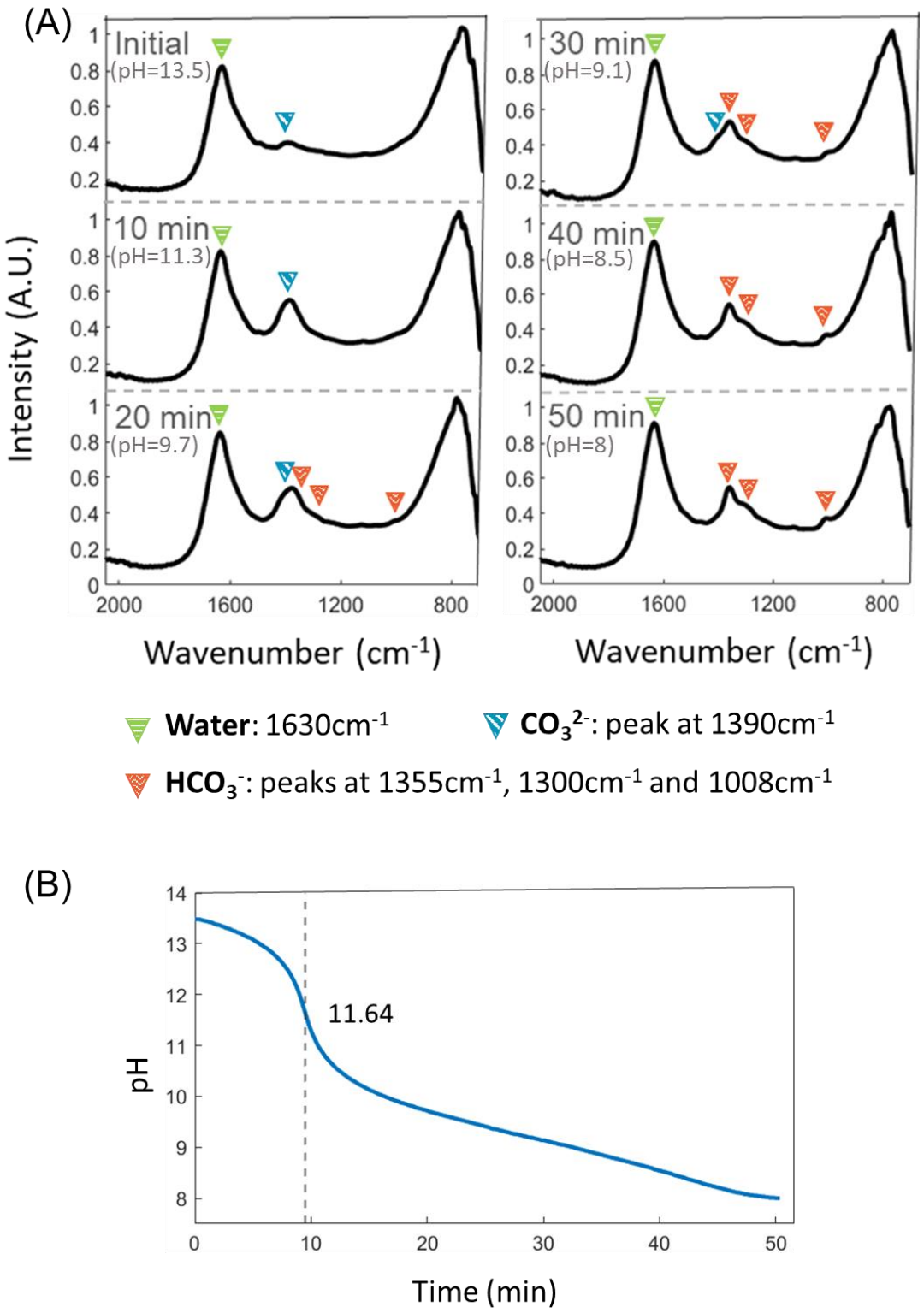

Figure 11. (A) FTIR spectra with time during a carbonation of black liquor. The bands marked with a green arrow at around 1630 cm-1 correspond to the absorbance of water, the bands marked with a blue arrow at 1390 cm-1 show the CO_3^{2-}, and the three bands in red color at 1355, 13000, and 1008 cm-1 are characteristic of HCO_3^-. (B) Evolution of pH with time during the carbonation of black liquor.

The same experimental approach was also attempted for aqueous mixtures of green liquor dregs and steelmaking slag. As can be seen in Figure 12A the FTIR spectra showed the formation of carbonates, by the appearance of peaks at around 1390 and 1008 cm^{-1}. The pH exhibited a fast drop to 8 and it did not follow the same trend of decline as in the other absorbents. This was an early indication that the carbonation had not been complete, which was confirmed when the experiment was repeated for the same duration with weight measurements. Figure 12C shows that the weight of the reactor was still displaying a steep increase at pH 8, which means that CO_2 was still being absorbed at a fast rate. Therefore, to avoid losing the information of capture capacity of the materials, experiments were conducted where the weight of the reactor was measured until it reached a stable value. The results of these experiments will be presented in section 4.3.

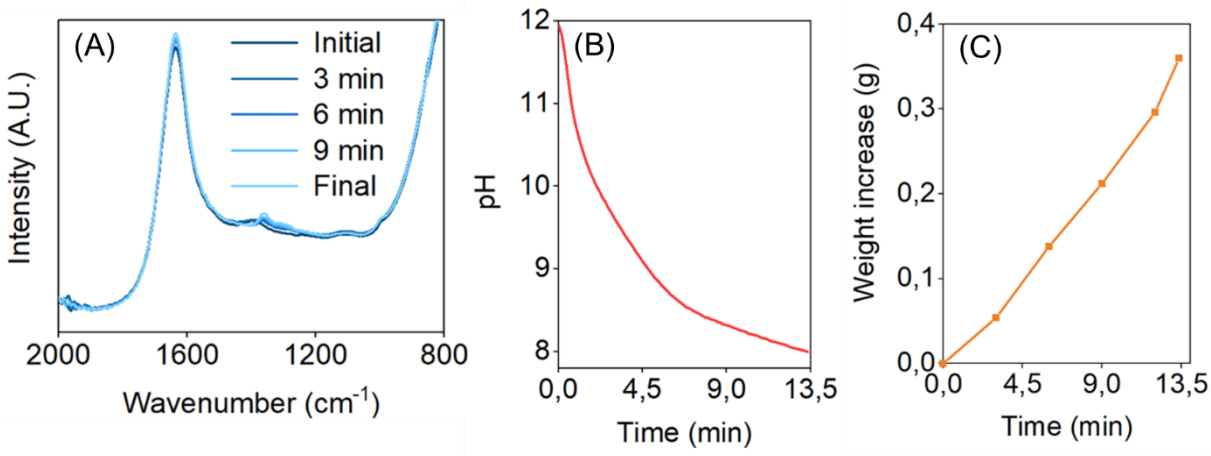

Figure 12. Initial experiment of green liquor dregs 15% where the experiment duration was dictated by the drop of pH to 8.

4.3. Absorption capacity

The absorption capacity is one of the most important parameters in carbon capture as it determines the amount of CO_2 that can be collected per volume of absorbent. Along with that, the absorption rate is also a significant factor that dictates the duration of the process. To investigate the effect of the concentration of NaOH in these properties an analytical balance was used to track the weight of the reactor during the gas flow for each solution. The weight of absorbed CO_2 overtime, along with the absorption yield in grams per liter of solution are presented for solutions of 1 w/w%, 4 w/w% and 8 w/w% of NaOH in Figure 13. As mentioned in section 3.2.3. the duration of these experiments was the same as the time it took for the pH to reach 8 in the previous series of experiments. The rate of absorption at the lowest concentration of NaOH (Figure 13A) was relatively stable throughout the duration of the experiment. The final CO_2 absorption reached after 4.3 minutes was 9.5 g/L. In the 4 w/w% solution, as discussed before, three distinct regions were identified with decreasing absorption

rates. The total CO_2 absorption there was 41.7 g/L after 61 min. For the solution with the highest concentration, there was an initial distinct region lasting for around 27 minutes with an absorption of almost 48 g/L while after that for the remaining 120 minutes of experiment the additional absorption was only 31 g/L. Interestingly, the maximum absorption obtained with the 4 w/w% solution after 61 minutes was reached in 1/3 of that time in the 8 w/w% solution.

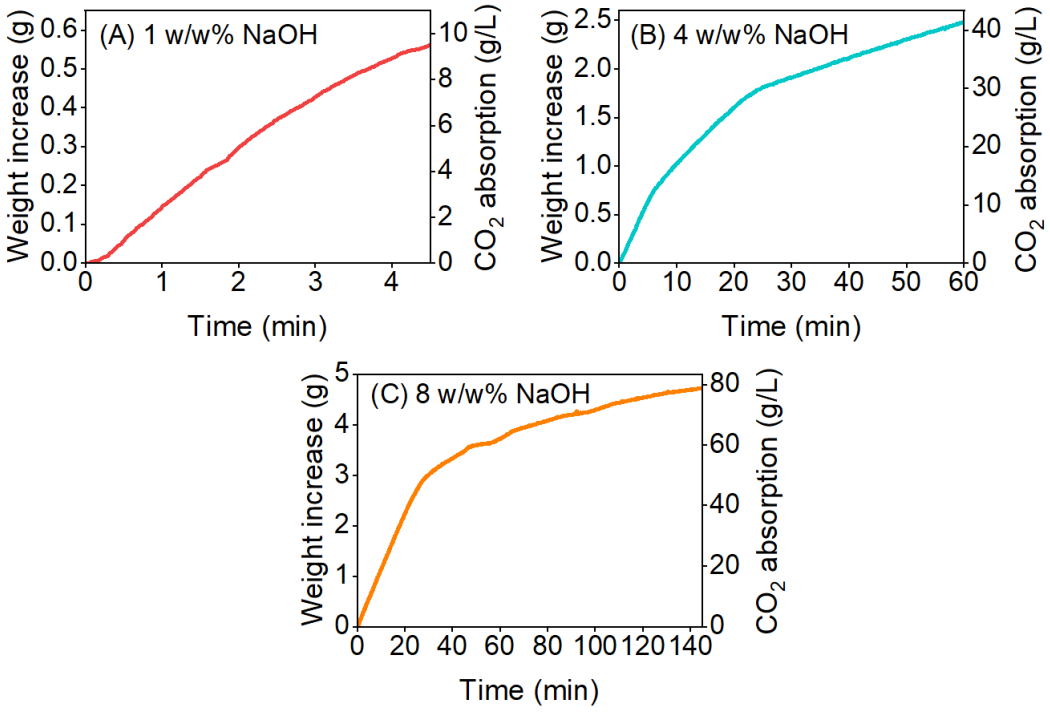

Figure 13. Weight increase of the reactor and the corresponding CO2 absorption for 1, 4 and 8 w/w% NaOH.

The absorption capacity of the NaOH solutions was compared to the stoichiometric amount of CO_2 that could react toward the formation of solely CO_3^{2-} or HCO_3^- as can be seen in Figure 14A. The absorption capacity values for all concentrations are near but not exactly identical to the theoretical capture with total conversion to bicarbonates. This suggests that HCO_3^- is the primary product of all experiments, but some CO_3^{2-} is also still present. The absorption capacity increases linearly with the concentration of NaOH as presented in Figure 14B. These results are in agreement with values reported in the literature, which further enhances the reliability of the designed setup [92].

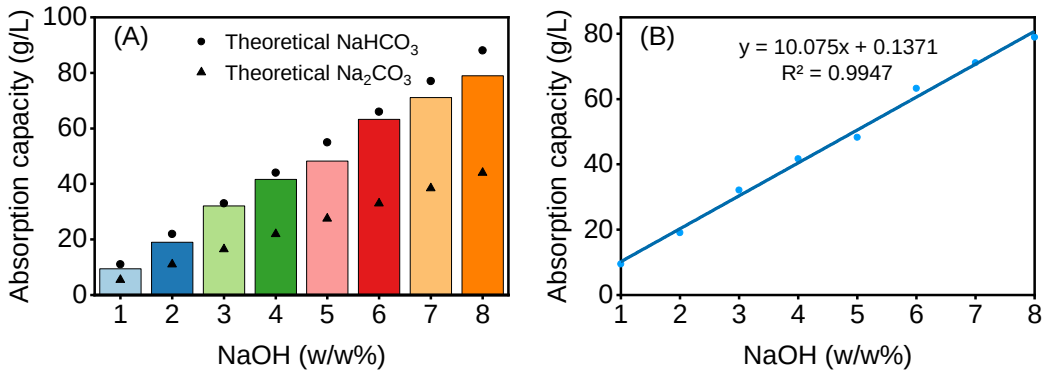

Figure 14. Obtained and theoretical absorption capacities for NaOH solutions of 1 to 8 w/w% NaOH. A total conversion of CO2 to carbonate and HCO_3^- was assumed to estimate the theoretical capacities using Eq 3 and 5 (A). Linear regression based on the experimental data, indicating that the concentration of NaOH and the absorption capacity correlate linearly (B).

The absorption capacity of CO_2 in weak oat black liquor is presented in Table 3. For the sake of reproducibility, the experiment was conducted in triplicate and the pH was measured at the end to ensure that it had reached the value of 8. All three experiments had the same duration and the final pH and absorption of CO_2 were almost the same. The average absorption capacity was 30.8 g of CO_2/L of black liquor, which according to Figure 14 corresponds to nearly 3 w/w% of an aqueous NaOH solution. The NaOH solution used during the cooking process of oat husks was 4 w/w%, but a small amount got carbonated in the cooking and some was lost in the filtration method to separate the pulp from the black liquor. The pulp is washed a few times with water to neutralize its pH and remove all lignin, but only the first filtrate was collected for the experiments, while the wash water was discarded. This loss is not significant, but in an industrial process, all of the wash water would be collected, and this weak black liquor could be condensed to a desirable content of NaOH before reacting with flue gas.

Table 3. Absorption capacity of CO_2 in black liquor.

Experiment No	Final pH	Absorption Capacity (g/L)
1	7.96	32.9
2	8.05	29.3
3	8.04	30.3

Figure 15 shows the evolution of absorption of CO_2 in green liquor dregs and steelmaking slags at different concentrations in water. In the pretreatment, the solids were mixed with water and stirred for 24 hours. Different stirring times were also tested and it was concluded that 24 hours were enough to obtain the maximum capacity of carbonation. As can be seen in Figure 16 with the comparison of all materials for one concentration, green liquor dregs were found to have the lowest

capture capacity. This is expected given that they contain less metal oxides than the steel slags. Surprisingly, Petrit T, which has the lowest concentration of CaO out of the three steelmaking slags and no MgO, had the highest absorption capacity. The effect of the particle size was not studied, but it is worth noting that Petrit T is fine powder, while Petrit E and L were coarser. The final pH of the carbonated mixtures was between 6.8 and 7.7.

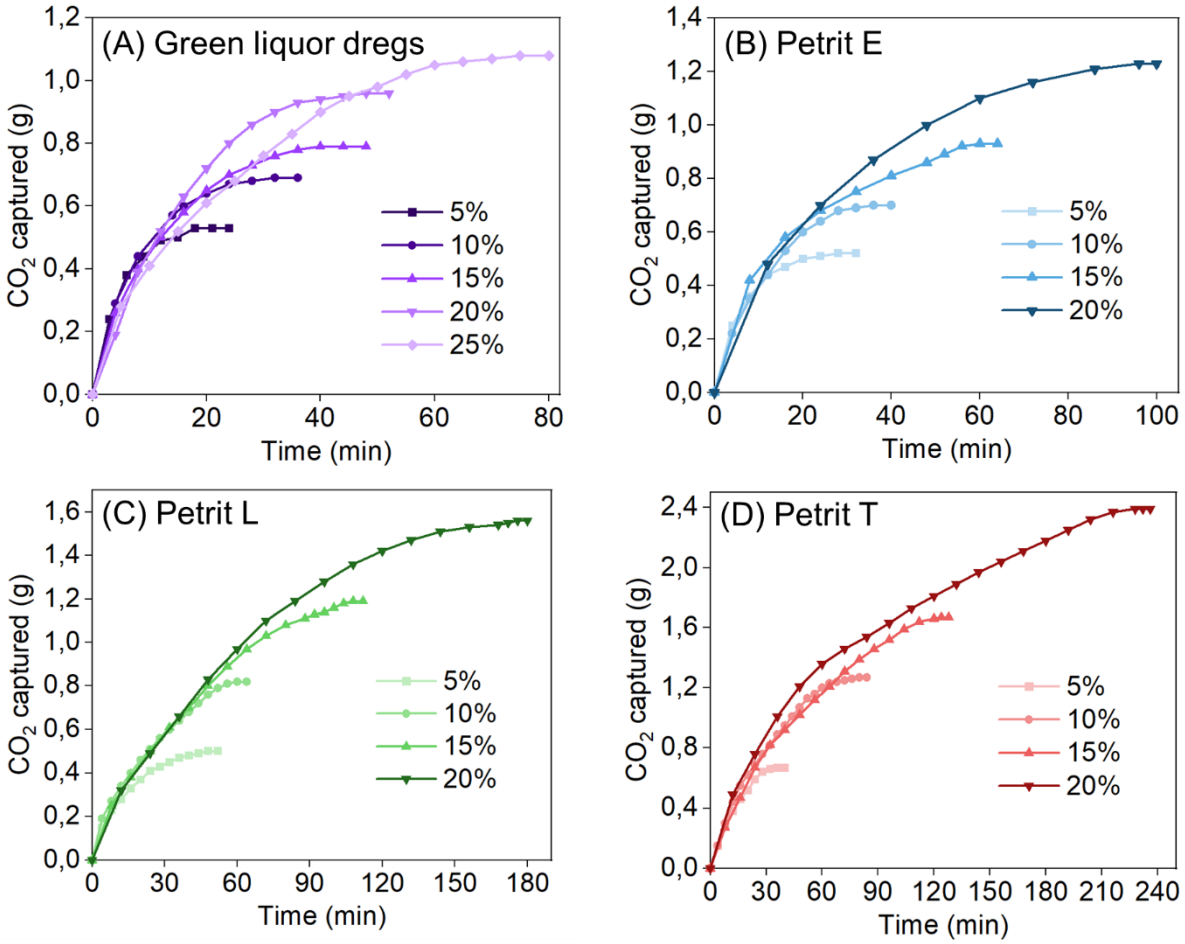

Figure 15. CO_2 captured evolution with time for (A) Green liquor dregs, (B) Petrit E, (C) Petrit L and (D) Petrit T.

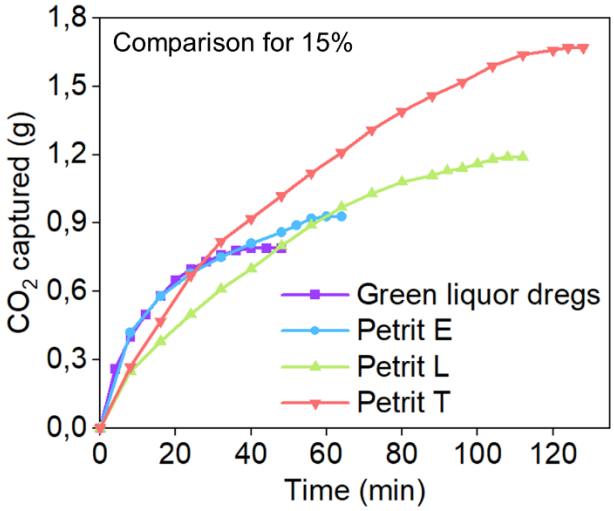

Figure 16. CO_2 captured evolution with time for all the materials at 15 w/v%.

It is obvious from Figure 15 that the absorption capacity increases with increasing concentration. The absorption yield of the materials, however, followed the opposite trend. It was observed that the degree of carbonation was higher for the lowest concentrations of solids in water. Figure 17 shows the capture capacity of the materials in terms of grams of CO_2 / L of mixture and grams of CO_2 / g of solid. The trend of the capture yield shows that the amount of CO_2 captured per gram of solid declined with increasing concentration. This phenomenon is related to the leaching of the metal ions. As the solid materials are mixed with water, metal ions leach out in the water until the equilibrium between the dissolved and solid species is reached. At high concentrations of solids, the water is quickly saturated with dissolved metal ions, while there are still metal oxide particles in the solid phase, thus this inhibition to leach more ions can make it more challenging to maximize the carbonation of the material. Based on this information it is clear that a golden ratio must be found between the optimum utilization of the materials and the volume of the reactor. Lower solid concentrations might yield higher carbonation, but they have lower absorption capacity and higher volume is required owing to the high water content. For the slags Petrit L and Petrit T there is only a mild drop in yield as the concentration increases so perhaps industrially it would be better to choose the 20 w/v% mixture, to ensure high absorption capacity with small reactor size. For the green liquor dregs and Petrit E there seems to be a bigger decline in yield between 5 and 10 w/v%, thus it would be less clear which is the optimum concentration. Of course, there are more parameters to be considered when designing such as process industrially, such as the clogging of the sparger, which is more intense for mixtures with higher solids content, the energy spent for the separation of water from the solids after the carbonation, etc.

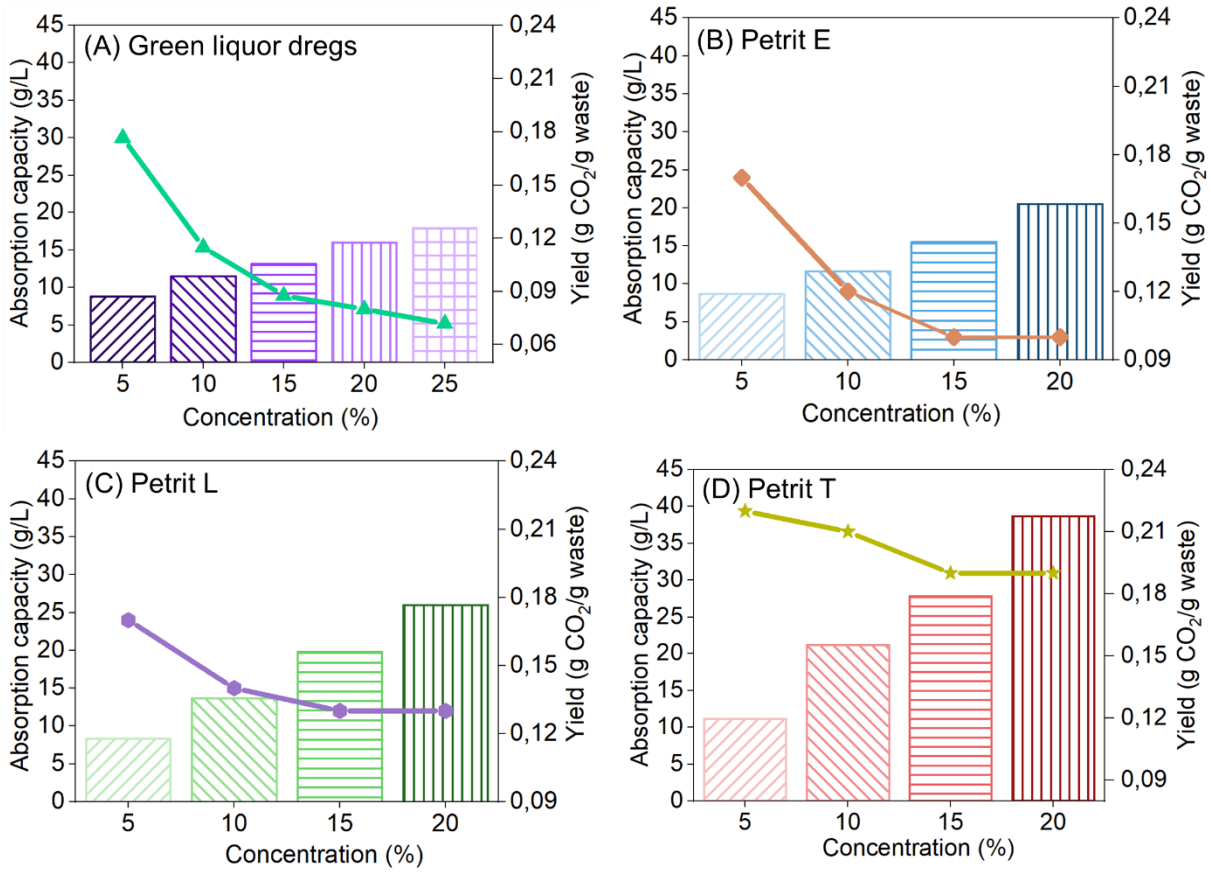

Figure 17. Absorption capacity and yield for (A) Green liquor dregs, (B) Petrit E, (C) Petrit L and (D) Petrit T.

4.4. Physicochemical characterization of the carbonates

The solids that precipitated from the 6 w/w% NaOH solution during the experiment were collected and analyzed with SEM and XRD. The crystals that formed with precipitation were organized in irregular, sharp structures of various shapes and sizes, as can be seen in the SEM images in Figure 18A-D. The XRD diffractogram of these crystals was also recorded (Figure 18E). According to the Crystallography Open Database, the patterns were recognized to belong primarily to natrite (main peaks at 26°, 27.5°, 33°, 35°, 38°, 40°, 41.5°, 46.5°, 47°, 48°, and all the other peaks from 53.5°), and to a minor extend to nahcolite (main peaks at 30°, 34.5°, and 44.5°).

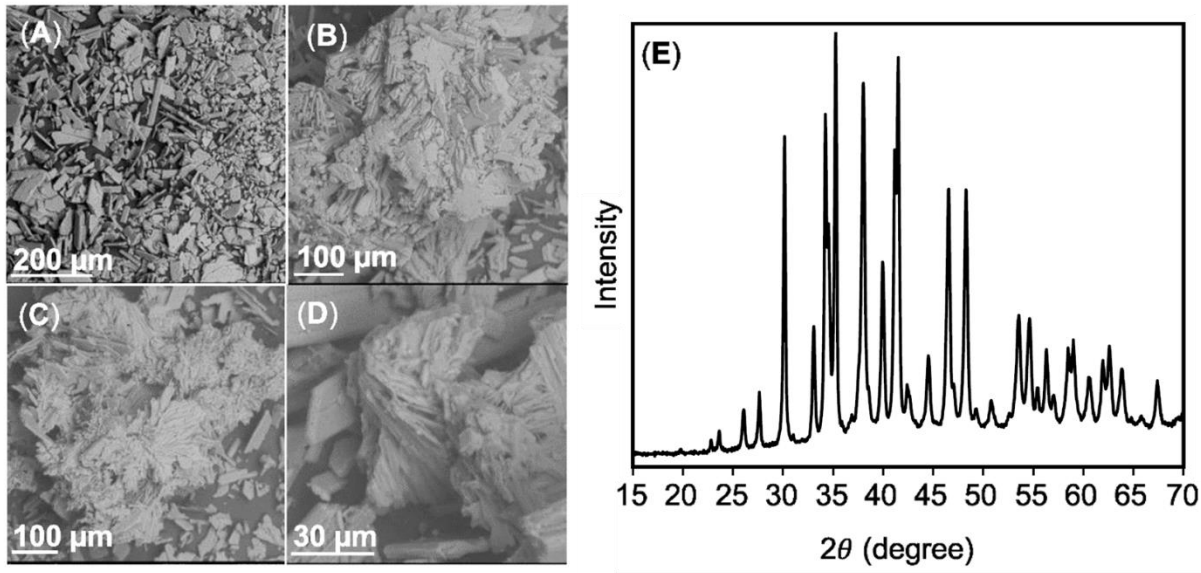

Figure 18. SEM images (A–D) and XRD diffractogram (E) of the powder obtained for 6 w/w% NaOH.

Samples of dried black liquor were prepared as described in 3.2.4. and analyzed with SEM, optical microscopy and XRD. The images from SEM and the optical microscope shown in Figure 19 can provide insight into the morphology and microstructures present in the material before and after carbonation. Black liquor, as can be seen in Figure 19A and E contains a variety of amorphous structures of mainly organic composition. As the pH of black liquor drops lignin molecules start to become insoluble and precipitate. The mechanism of precipitation is highly complex and maximum recovery of lignin can be achieved at pH between 2-3 [69]. At the pH of 8 a noticeable fraction of lignin had precipitated. If the raw lignocellulosic feedstock contains silica, this will also be present in black liquor in the form of soluble silicate ions, which turn into silica and precipitate at the pH range of 10-8 [93]. Thus, after carbonation, the filtration residue displayed in Figure 19B and F contains mainly lignin and silica, which are absent in the filtrate. Owing to this, the white, sharp crystals that appeared in the images of the filtrate could be assumed to be carbonates.

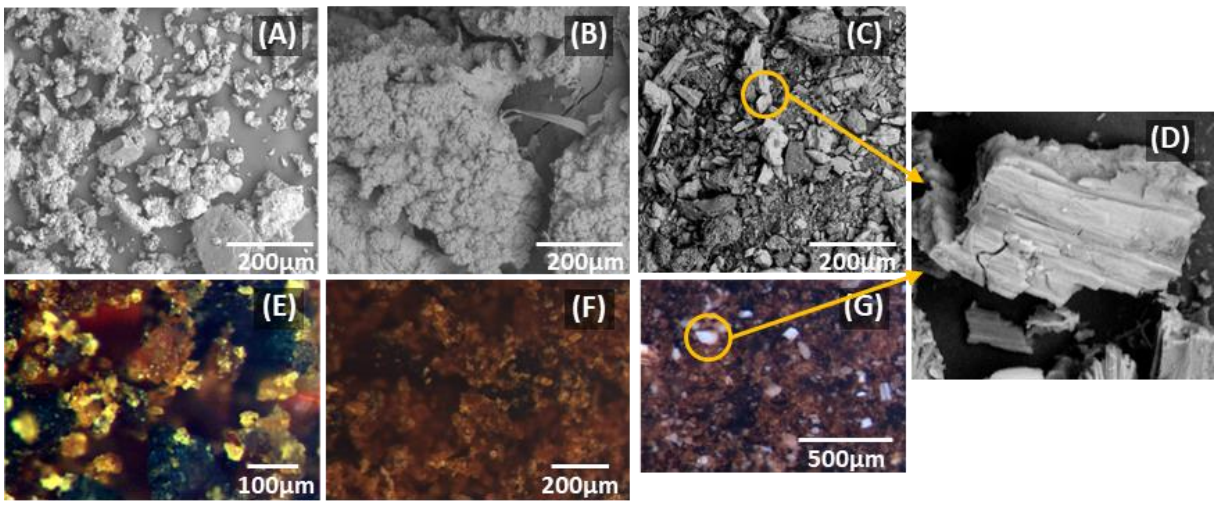

Figure 19. SEM images of (A) non-carbonated black liquor, (B) residue from the filtration of carbonated black liquor, (C) filtrate from the filtration of carbonated black liquor, (D) zoomed-in image of crystal from the filtrate and optical microscope images from (E) non-carbonated black liquor, (F) residue from the filtration of carbonated black liquor and (G) filtrate from the filtration of carbonated black liquor.

The XRD results (Figure 20) corroborate the microscopy images. While it is challenging to identify any known structures, especially in untreated black liquor (Figure 20A), it was possible to recognize patterns of carbonates in the residue and filtrate of the carbonated liquor. In Figure 20B a series of small peaks at the angle range of 32-60° had a 30% match to Na_2CO_3, according to the Figure of Merit (FOM) calculated in the XRD software. The broad band at smaller angles could correspond to amorphous silica as it has been previously reported in the literature [94]–[96]. In the diffractogram of the filtrate the presence of carbonates was more pronounced as there was a 55% match of the pattern to Na_2CO_3 and a 13% match to $NaHCO_3$ according to the FOM (Figure 20C). The FOM does not provide quantitative information. It is an expression of how well the pattern of the recorded signal fits to the diffractograms of model molecular structures stored in the Crystallography Open Database.

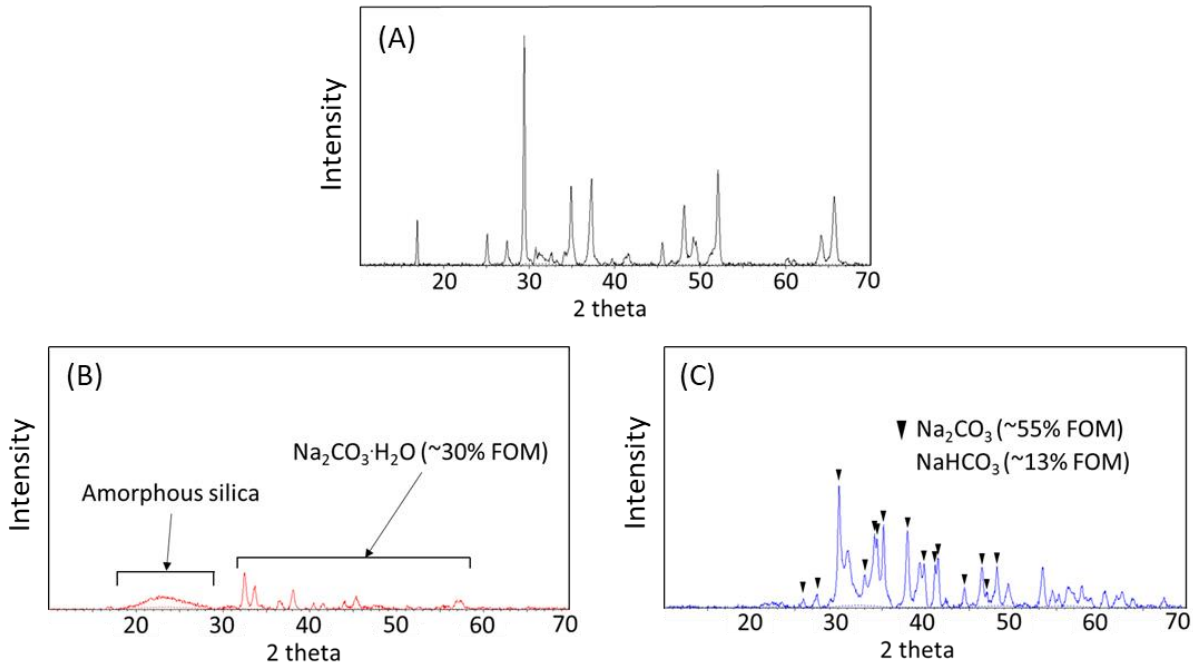

Figure 20. XRD diffractograms of black liquor (A), non-carbonated residue from the filtration of carbonated black liquor (B), and filtrate from the filtration of carbonated black liquor (C). The Figure of Merit (FOM) displayed in (B) and (C) is an indication of how much the signal matches with that of a particular molecular structure from the Crystallography Open Database.

The black liquor was also analyzed with NMR before and after carbonation (Figure 21). The peaks in the region 50–100 ppm belong most likely to hemicelluloses. Peaks that are characteristic of lignin appear typically at the range of 100-120 ppm for the aromatic groups of lignin and at 50 ppm for the methoxy groups, but these were not present in the spectra. However, the NMR spectrum for the black liquor before carbonation (Figure 21A) showed almost no lignin peaks. This might be due to the low amount of lignin. The peak at 168 ppm corresponds to CO_3^{2-} confirming that the non-carbonated black liquor contains a small amount of CO_3^{2-} which agrees with the FTIR results. After carbonation at pH 8, there was no considerable change in the signal coming from organic molecules (Figure 21B). However, the CO_3^{2-} peak disappeared, and another more intense peak at 161 ppm corresponding to HCO_3^- appeared [97]. This indicates that the black liquor had been carbonated, and the dominant species are bicarbonates which is reasonable at pH 8.

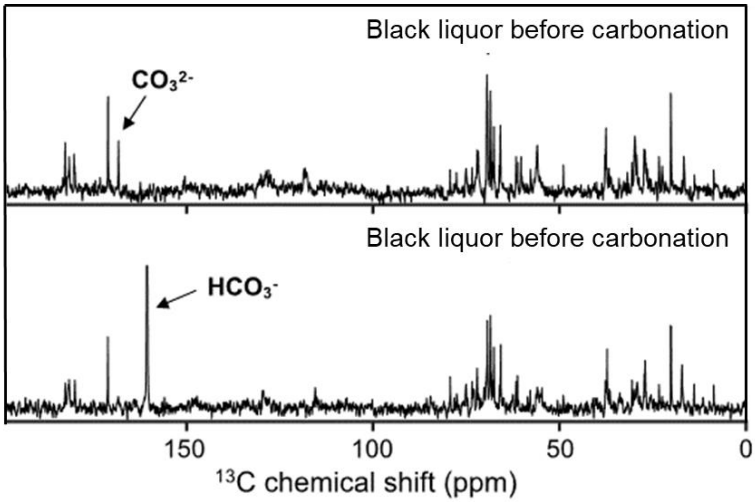

Figure 21. Liquid state ^{13}C NMR spectra of black liquor before carbonation (A) and after carbonation (B and C). B and C are two different runs.

For the green liquor dregs, SEM analysis revealed the complex morphology of the material (Figure 22). There was a variety of crystalline and amorphous structures both before and after carbonation. Tetrahedral structures that were identified in the samples before and after carbonation could indicate the presence of calcite [98]. Such structures are clearly visible in Figures 23B and D. An interesting phenomenon that appeared during the experiments is that for the high concentrations of green liquor dregs (20 and 25 w/v%) crystalline structures were forming on the surface of the solids after the carbonation experiments. These crystals were isolated and then analyzed with SEM as well. Elemental analysis with SEM revealed that the crystals contained Mg (13%), C (17.7%) and O (69.4%). The morphology of one of these crystals can be seen in Figure 23.

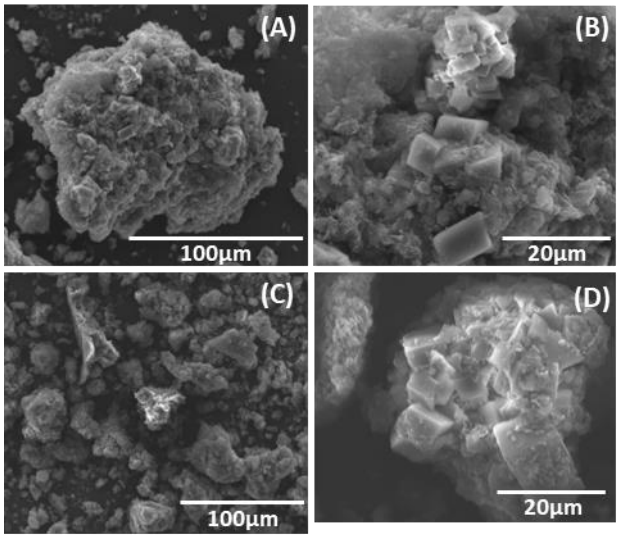

Figure 22. SEM images of green liquor dregs before (A and B) and after (C and D) carbonation. The carbonated sample is the one from the experiment at 5 w/v% concentration.

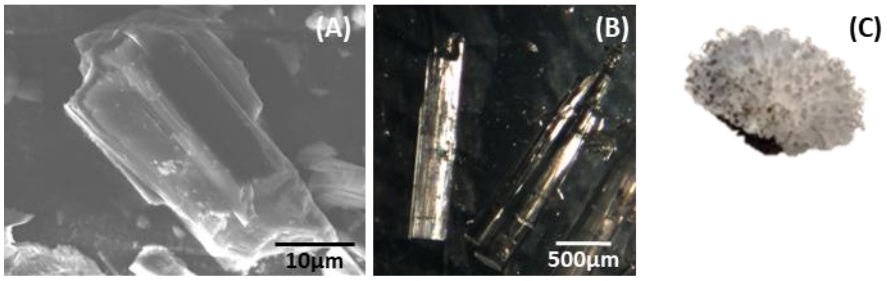

Figure 23. Crystal structure formed on the surface of the carbonates green liquor dregs at 25 w/v% as seen with (A) SEM, (B) the optical microscope. (C) is a picture of the crystal.

XRD analysis (Figure 24) showed that the most predominant structure in the green liquor dregs was $CaCO_3$ already before the carbonation, which has also been reported in the literature [99]–[101]. Specifically, the XRD patterns match the crystal phase structure of calcite [102], [103]. A peak at 26.15 has been identified to belong to manganite (MnO(OH)) [99]. This peak appears unchanged before and after carbonation for low and high concentrations of green liquor dregs, while the peaks of $CaCO_3$ are higher after carbonation and specifically, the maximum intensity appeared at the concentration of 5 w/v%. This confirms the notion that more $CaCO_3$ was formed in the experiment with 5 w/v% solids, than with 25 w/v%.

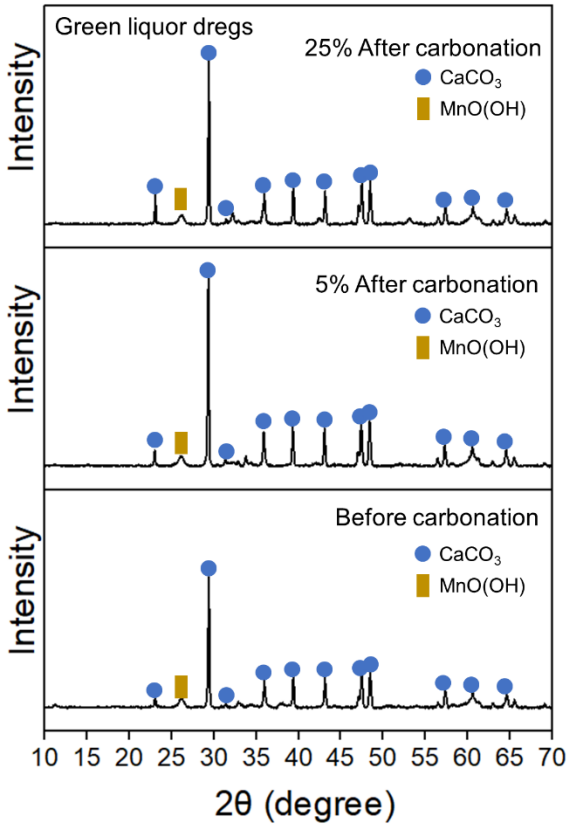

Figure 24. XRD diffractograms of green liquor dregs before carbonation and after for mixtures 5 and 25 w/v%.

The morphology of the steelmaking slags as observed with SEM can be seen in Figure 25. The morphology of the samples before carbonation (Figure 25A, C and E) is different among the virgin slags. For example, the particles of Petrit E had a rock-like shape, while Petrit T had more of a sponge-like morphology. The carbonated samples showed more similarities between them (Figure 25B, D and F). According to previous references, calcite presents a tetrahedral morphology. A tetrahedral morphology could be recognized in Figure 25B (carbonated petrit E) and F (carbonated Petrit T), which could belong to calcite as was mentioned above [98]. For the carbonated sample of Petrit L, a mix between tetrahedral and needle-like structures was observed (Figure 25D). This could correspond to a mix of calcite and aragonite or $MgCO_3$, in agreement with previous works [104], [105].

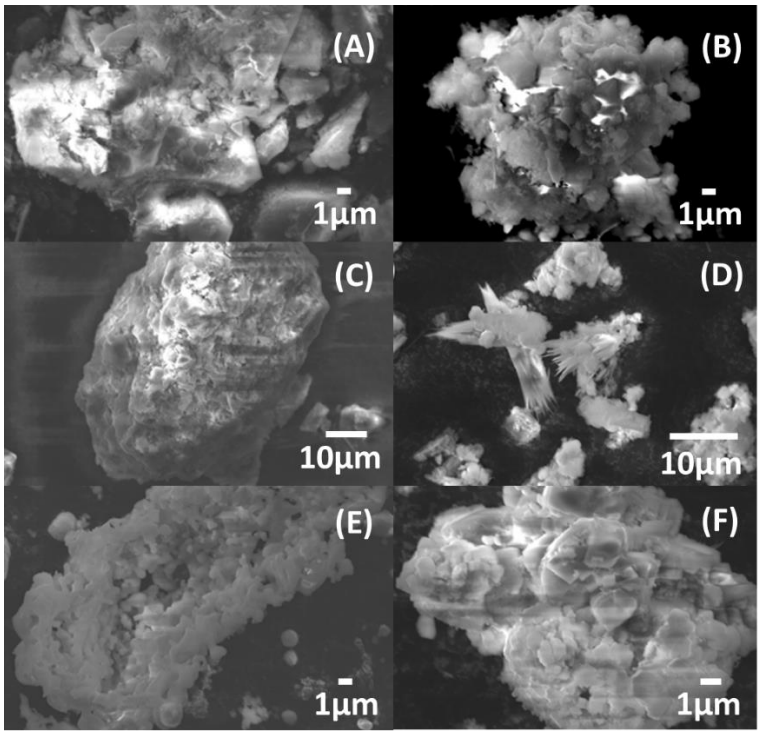

Figure 25. SEM of solid powders for: (A) Petrit E before carbonation; (B) Petrit E after carbonation; (C) Petrit L before carbonation; (D) Petrit L after carbonation; (E) Petrit T before carbonation; (F) Petrit T after carbonation. The carbonated samples are the ones from the experiment at 15 w/v% concentration.

XRD unveiled the mixture of metal complexes that these materials comprise (Figure 26). Before carbonation a variety of metal oxides and silicates could be recognized based on the Crystallography Open Database. Petrit E and L had peaks characteristic of Ca_2SiO_4, $CaCO_3$ and MgO before carbonation. Petrit T displayed a strong presence of Ca_2SiO_4, but there was no indication of $CaCO_3$, while CaO could be identified. This can explain why Petrit T had the highest carbonation performance, since Ca^+ were more readily available to react. After the carbonation reactions calcite had the most predominant signal, while peaks of $MgCO_3$ were also visible in Petrit E and L. The high

content of carbonates after the experiments suggests that these materials might be attractive for use in constructions.

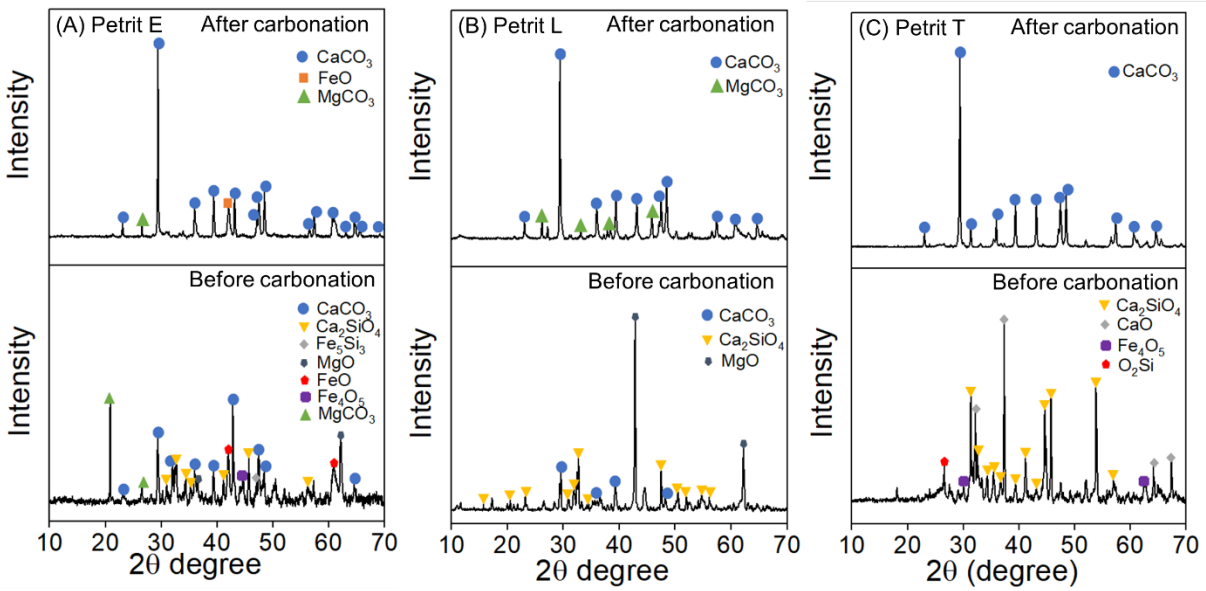

Figure 26. XRD diffractograms of (A) Petrit E, (B) Petrit L and (C) Petrit T, before and after carbonation.

5. Conclusions

The following absorption systems have been studied in terms of their potential in carbon capture: aqueous NaOH, black liquor, aqueous green liquor dregs and aqueous steelmaking slags.

Experiments were conducted in a bubble column reactor which was designed to have a narrow body in order to induce homogeneous mixing of the gas and liquid phase by the upward movement of the gas bubbles, without the need for stirring. This setup was validated with the use of standard solutions of NaOH and it was then used for the carbonation experiments of green liquor dregs and steelmaking slags. Black liquor contains various molecules which act as surfactants and thus it tends to form a dense foam when gas is sparged through it. To restrain the foam, a stirred tank was used instead of a bubble column and the stirrer was operated at the elevated speed of 700 rpm which was successful at breaking the foam at the rate of its production.

It was found that black liquor had a capture capacity of 30.8 g of CO_2 / L of liquor, which however is largely dependent on the solids content of the weak liquor and the amount of NaOH used in the cooking process. A fraction of lignin and silica present in the liquor precipitated as a result of lowering the pH. Green liquor dregs and steelmaking slags were mixed with water at different concentrations and stirred for 24 hours to promote the leaching of metal ions. It was found that concentration is a crucial parameter affecting the absorption capacity. At higher concentrations of solids, the absorption capacity was higher, but the degree of carbonation of the solids was lower. Out of all the side-streams tested the steel slag Petrit T had the highest absorption of CO_2 owing to its high content in readily available CaO. While Petrit E and Petrit L had more CaO according to the chemical analysis provided by the supplier, XRD revealed that the Ca partially existed in the form of $CaCO_3$.

6. Future perspectives

The next steps in this project are two-fold. The first part is to expand the research on more industrial side-streams, such as a waste-water stream provided by SCA and municipal bottom ash from Uddevalla Energi. To this end the experimental setup has been modified in the following ways: 1) the gas composition will be adjustable with a mass flow controller and will be set to 15 % of CO_2 to be more representative of post-combustion flue gas, 2) a CO_2 sensor will be measuring the % of CO_2 in the outlet of the reactor. Thus, by collecting data on the composition of the outlet it will be possible to deduct the amount of CO_2 that is absorbed in the reactor over time. In this way it will be possible to study different side-streams, experimental conditions and reactor designs. This part also includes the prospect of analyzing the properties of the carbonated materials to evaluate potential utilization paths.

The second part entails the visualization of the flow field inside the bubble column reactor using Magnetic Resonance Imaging (MRI). MRI is a powerful methodology to gain crucial information of opaque systems by detecting the signal coming from ^1H and constructing flow or other maps. This technique is primarily used in medicine, but it is emerging fast in the chemical engineering world and one of its promising applications is for flow visualization and reaction monitoring inside multiphase reactors. While high speed cameras can provide insight transparent systems such as bubble columns with water and air, they fail when the liquid phase is opaque. That is where MRI comes in. The main challenge of this technique is to develop methods that will be fast enough to capture the movement of the bubbles inside the liquid in time-scales below seconds. If this is achieved then it will be possible to obtain information about the flow inside black liquor, mixtures of solid materials in water and other opaque systems. This information can then be used to corroborate the construction of accurate CFD models, which could be useful for large-scale implementation.

7. References

[1] S. Manabe, 'Role of greenhouse gas in climate change', *Tellus A: Dynamic Meteorology and Oceanography*, vol. 71, no. 1, p. 1620078, Jan. 2019, doi: 10.1080/16000870.2019.1620078.

[2] 'Overview of Greenhouse Gases, EPA', https://www.epa.gov/ghgemissions/overview-greenhouse-gases.

[3] K. Calvin *et al.*, 'IPCC, 2023: Climate Change 2023: Synthesis Report. Contribution of Working Groups I, II and III to the Sixth Assessment Report of the Intergovernmental Panel on Climate Change [Core Writing Team, H. Lee and J. Romero (eds.)]. IPCC, Geneva, Switzerland.', Jul. 2023. doi: 10.59327/IPCC/AR6-9789291691647.

[4] P. Goglio *et al.*, 'Advances and challenges of life cycle assessment (LCA) of greenhouse gas removal technologies to fight climate changes', *J Clean Prod*, vol. 244, p. 118896, Jan. 2020, doi: 10.1016/j.jclepro.2019.118896.

[5] Z. Zhang *et al.*, 'Advances in carbon capture, utilization and storage', *Appl Energy*, vol. 278, p. 115627, Nov. 2020, doi: 10.1016/j.apenergy.2020.115627.

[6] A. Dubey and A. Arora, 'Advancements in carbon capture technologies: A review', *J Clean Prod*, vol. 373, p. 133932, Nov. 2022, doi: 10.1016/j.jclepro.2022.133932.

[7] Y. Peng, B. Zhao, and L. Li, 'Advance in Post-Combustion CO_2 Capture with Alkaline Solution: A Brief Review', *Energy Procedia*, vol. 14, pp. 1515–1522, 2012, doi: 10.1016/j.egypro.2011.12.1126.

[8] I. Sreedhar, T. Nahar, A. Venugopal, and B. Srinivas, 'Carbon capture by absorption – Path covered and ahead', *Renewable and Sustainable Energy Reviews*, vol. 76, pp. 1080–1107, Sep. 2017, doi: 10.1016/j.rser.2017.03.109.

[9] U. Desideri, 'Advanced absorption processes and technology for carbon dioxide (CO_2) capture in power plants', in *Developments and Innovation in Carbon Dioxide (CO2) Capture and Storage Technology*, Elsevier, 2010, pp. 155–182. doi: 10.1533/9781845699574.2.155.

[10] E. S. Rubin, H. Mantripragada, A. Marks, P. Versteeg, and J. Kitchin, 'The outlook for improved carbon capture technology', *Prog Energy Combust Sci*, vol. 38, no. 5, pp. 630–671, Oct. 2012, doi: 10.1016/j.pecs.2012.03.003.

[11] T. Nguyen, M. Hilliard, and G. T. Rochelle, 'Amine volatility in CO_2 capture', *International Journal of Greenhouse Gas Control*, vol. 4, no. 5, pp. 707–715, Sep. 2010, doi: 10.1016/j.ijggc.2010.06.003.

[12] B. Zhao *et al.*, 'Study on corrosion in CO_2 chemical absorption process using amine solution', *Energy Procedia*, vol. 4, pp. 93–100, 2011, doi: 10.1016/j.egypro.2011.01.028.

[13] H. Leifsen, 'Post-Combustion CO_2 Capture Using Chemical Absorption Minimizing Energy Requirement. Master of Science in Energy and Environment', 2007.

[14] A. B. Rao and E. S. Rubin, 'A Technical, Economic, and Environmental Assessment of Amine-Based CO $_2$ Capture Technology for Power Plant Greenhouse Gas Control', *Environ Sci Technol*, vol. 36, no. 20, pp. 4467–4475, Oct. 2002, doi: 10.1021/es0158861.

[15] P. V. Danckwerts and A. M. Kennedy, 'The kinetics of absorption of carbon dioxide into neutral and alkaline solutions', *Chem Eng Sci*, vol. 8, no. 3–4, pp. 201–215, Jun. 1958, doi: 10.1016/0009-2509(58)85027-7.

[16] R. Pohorecki and W. Moniuk, 'Kinetics of reaction between carbon dioxide and hydroxyl ions in aqueous electrolyte solutions', *Chem Eng Sci*, vol. 43, no. 7, pp. 1677–1684, 1988, doi: 10.1016/0009-2509(88)85159-5.

[17] L. Kucka, E. Y. Kenig, and A. Górak, 'Kinetics of the Gas–Liquid Reaction between Carbon Dioxide and Hydroxide Ions', *Ind Eng Chem Res*, vol. 41, no. 24, pp. 5952–5957, Nov. 2002, doi: 10.1021/ie020452f.

[18] S. Gondal, N. Asif, H. F. Svendsen, and H. Knuutila, 'Kinetics of the absorption of carbon dioxide into aqueous hydroxides of lithium, sodium and potassium and blends of hydroxides and carbonates', *Chem Eng Sci*, vol. 123, pp. 487–499, Feb. 2015, doi: 10.1016/j.ces.2014.10.038.

[19] G. Astarita, 'Absorption of Carbon Dioxide into Alkaline Solutions in Packed Towers', *Industrial & Engineering Chemistry Fundamentals*, vol. 2, no. 4, pp. 294–297, Nov. 1963, doi: 10.1021/i160008a009.

[20] D. Santa Cruz-Navarro, V. Mugica-Álvarez, M. Gutiérrez-Arzaluz, and M. Torres-Rodríguez, 'CO_2 Capture by Alkaline Carbonation as an Alternative to a Circular Economy', *Applied Sciences*, vol. 10, no. 3, p. 863, Jan. 2020, doi: 10.3390/app10030863.

[21] W. Kordylewski, D. Sawicka, and T. Falkowski, 'Laboratory tests on the efficiency of carbon dioxide capture from gases in NaOH solutions', *Journal of Ecological Engineering*, vol. 14, no. 2, pp. 54–62, Apr. 2013, doi: 10.5604/2081139X.1043185.

[22] E. R. Bobicki, Q. Liu, Z. Xu, and H. Zeng, 'Carbon capture and storage using alkaline industrial wastes', *Prog Energy Combust Sci*, vol. 38, no. 2, pp. 302–320, Apr. 2012, doi: 10.1016/j.pecs.2011.11.002.

[23] P. Renforth, 'The negative emission potential of alkaline materials', *Nat Commun*, vol. 10, no. 1, p. 1401, Mar. 2019, doi: 10.1038/s41467-019-09475-5.

[24] S.-Y. Pan, K. J. Shah, Y.-H. Chen, M.-H. Wang, and P.-C. Chiang, 'Deployment of Accelerated Carbonation Using Alkaline Solid Wastes for Carbon Mineralization and Utilization Toward a Circular Economy', *ACS Sustain Chem Eng*, vol. 5, no. 8, pp. 6429–6437, Aug. 2017, doi: 10.1021/acssuschemeng.7b00291.

[25] J. S. Cho, S. M. Kim, H. D. Chun, G. W. Han, and C. H. Lee, 'Carbon Dioxide Capture with Accelerated Carbonation of Industrial Combustion Waste', *International Journal of Chemical Engineering and Applications*, pp. 60–65, 2011, doi: 10.7763/IJCEA.2011.V2.76.

[26] F. Bonfante, G. Ferrara, P. Humbert, J.-M. Tulliani, and P. Palmero, 'Direct Aqueous Mineralization of Industrial Waste for the Production of Carbonated Supplementary Cementitious Materials', 2023, pp. 581–592. doi: 10.1007/978-3-031-33187-9_54.

[27] J. Pedraza, A. Zimmermann, J. Tobon, R. Schomäcker, and N. Rojas, 'On the road to net zero-emission cement: Integrated assessment of mineral carbonation of cement kiln dust', *Chemical Engineering Journal*, vol. 408, p. 127346, Mar. 2021, doi: 10.1016/j.cej.2020.127346.

[28] Z. Chen, Z. Cang, F. Yang, J. Zhang, and L. Zhang, 'Carbonation of steelmaking slag presents an opportunity for carbon neutral: A review', *Journal of CO2 Utilization*, vol. 54, p. 101738, Dec. 2021, doi: 10.1016/j.jcou.2021.101738.

[29] T.-L. Chen, Y.-H. Chen, M.-Y. Dai, and P.-C. Chiang, 'Stabilization-solidification-utilization of MSWI fly ash coupling CO_2 mineralization using a high-gravity rotating packed bed', *Waste Management*, vol. 121, pp. 412–421, Feb. 2021, doi: 10.1016/j.wasman.2020.12.031.

[30] R. Baciocchi, G. Costa, E. Di Bartolomeo, A. Polettini, and R. Pomi, 'The effects of accelerated carbonation on CO_2 uptake and metal release from incineration APC residues', *Waste Management*, vol. 29, no. 12, pp. 2994–3003, Dec. 2009, doi: 10.1016/j.wasman.2009.07.012.

[31] 'Mineral Commodity Summaries 2022 - Iron and Steel Slag'.

[32] A. Dwivedi and M. K. Jain, 'Fly ash-waste management and overview : A Review', *Recent Research in Science and Technology*, vol. 6, no. 1, pp. 30–35, 2014.

[33] C. H. Kim, J. Y. Lee, S. H. Park, and S. O. Moon, 'Global trends and prospects of black liquor as bioenergy', *Palpu Chongi Gisul/Journal of Korea Technical Association of the Pulp and Paper Industry*, vol. 51, no. 5, pp. 3–15, Sep. 2019, doi: 10.7584/JKTAPPI.2019.10.51.5.3.

[34] A. Parbhakar-Fox, K. Bhowany, K. Guerin, L. Jackson, and P. Narayan Mishra, 'Tapping mineral wealth in mining waste could offset damage from new green economy mines'. Accessed: Nov. 01, 2023. [Online]. Available: https://theconversation.com/tapping-mineral-wealth-in-mining-waste-could-offset-damage-from-new-green-economy-mines-183232

[35] N. Zhang, H. Duan, T. R. Miller, V. W. Y. Tam, G. Liu, and J. Zuo, 'Mitigation of carbon dioxide by accelerated sequestration in concrete debris', *Renewable and Sustainable Energy Reviews*, vol. 117, p. 109495, Jan. 2020, doi: 10.1016/j.rser.2019.109495.

[36] J. C. Lee, S. L. Bradshaw, T. B. Edil, and C. H. Benson, 'Quantifying the Benefits of Using Flue Gas Desulfurization Gypsum in Sustainable Wallboard Production', *Coal Combustion and Gasification Products*, vol. 4, no. 1, pp. 17–20, 2012, doi: 10.4177/CCGP-D-11-00007.1.

[37] S.-J. Han and J.-H. Wee, 'Carbon Dioxide Fixation via the Synthesis of Sodium Ethyl Carbonate in NaOH-Dissolved Ethanol', *Ind Eng Chem Res*, vol. 55, no. 46, pp. 12111–12118, Nov. 2016, doi: 10.1021/acs.iecr.6b03250.

[38] S.-J. Mun, S.-J. Han, and J.-H. Wee, 'Carbon Dioxide Fixation by Precipitating $NaHCO_3$ via Carbonation of NaOH-Dissolved Ethanol Aqueous Solution', *Energy & Fuels*, vol. 32, no. 8, pp. 8614–8622, Aug. 2018, doi: 10.1021/acs.energyfuels.8b01584.

[39] J. Pak, S.-J. Han, and J.-H. Wee, 'Precipitation of potassium-based carbonates for carbon dioxide fixation via the carbonation and re-carbonation of KOH dissolved aqueous ethanol solutions', *Chemical Engineering Journal*, vol. 427, p. 131669, Jan. 2022, doi: 10.1016/j.cej.2021.131669.

[40] S.-J. Han and J.-H. Wee, 'Carbon Dioxide Fixation by Combined Method of Physical Absorption and Carbonation in NaOH-Dissolved Methanol', *Energy & Fuels*, vol. 31, no. 2, pp. 1747–1755, Feb. 2017, doi: 10.1021/acs.energyfuels.6b02709.

[41] R. Niu, C. Wu, B. Yue, N. Song, and Q. Wang, 'Estimation and prediction of the generation of waste organic solvents in China', *J Mater Cycles Waste Manag*, vol. 22, no. 4, pp. 1094–1102, Jul. 2020, doi: 10.1007/s10163-020-01002-9.

[42] P. K. W. Lau and A. Koenig, 'Management, disposal and recycling of waste industrial organic solvents in Hong Kong', *Chemosphere*, vol. 44, no. 1, pp. 9–15, Jul. 2001, doi: 10.1016/S0045-6535(00)00378-7.

[43] S. Evans, 'Around the world in 22 carbon capture projects'. Accessed: Oct. 15, 2023. [Online]. Available: https://www.carbonbrief.org/around-the-world-in-22-carbon-capture-projects/

[44] 'National Center for Biotechnology Information. PubChem Compound Summary for CID 14798, Sodium Hydroxide'. Accessed: Oct. 17, 2023. [Online]. Available: https://pubchem.ncbi.nlm.nih.gov/compound/Sodium-Hydroxide

[45] J.-G. Shim, D. W. Lee, J. H. Lee, and N.-S. Kwak, 'Experimental study on capture of carbon dioxide and production of sodium bicarbonate from sodium hydroxide', *Environmental Engineering Research*, vol. 21, no. 3, pp. 297–303, Sep. 2016, doi: 10.4491/eer.2016.042.

[46] Y. Tavan and S. H. Hosseini, 'A novel rate of the reaction between NaOH with CO_2 at low temperature in spray dryer', *Petroleum*, vol. 3, no. 1, pp. 51–55, Mar. 2017, doi: 10.1016/j.petlm.2016.11.006.

[47] M. Krauβ and R. Rzehak, 'Reactive absorption of CO_2 in NaOH: Detailed study of enhancement factor models', *Chem Eng Sci*, vol. 166, pp. 193–209, Jul. 2017, doi: 10.1016/j.ces.2017.03.029.

[48] C. E. Giacomin, 'Fluidized calcium carbonate crystallization in alkaline liquids', 2019.

[49] 'National Center for Biotechnology Information. PubChem Compound Summary for CID 767, Carbonic Acid.' Accessed: Oct. 19, 2023. [Online]. Available: https://pubchem.ncbi.nlm.nih.gov/compound/Carbonic-Acid

[50] 'National Center for Biotechnology Information. PubChem Compound Summary for CID 10340, Sodium Carbonate'. Accessed: Oct. 19, 2023. [Online]. Available: https://pubchem.ncbi.nlm.nih.gov/compound/Sodium-Carbonate

[51] 'National Center for Biotechnology Information. PubChem Compound Summary for CID 516892, Sodium Bicarbonate'. Accessed: Oct. 19, 2023. [Online]. Available: https://pubchem.ncbi.nlm.nih.gov/compound/Sodium-Bicarbonate

[52] P. Bajpai, 'Basic Overview of Pulp and Paper Manufacturing Process', in *Green Chemistry and Sustainability in Pulp and Paper Industry*, Cham: Springer International Publishing, 2015, pp. 11–39. doi: 10.1007/978-3-319-18744-0_2.

[53] A. Haile *et al.*, 'Pulp and paper mill wastes: utilizations and prospects for high value-added biomaterials', *Bioresour Bioprocess*, vol. 8, no. 1, p. 35, Apr. 2021, doi: 10.1186/s40643-021-00385-3.

[54] T. Kinnarinen, M. Golmaei, E. Jernström, and A. Häkkinen, 'Separation, treatment and utilization of inorganic residues of chemical pulp mills', *J Clean Prod*, vol. 133, pp. 953–964, Oct. 2016, doi: 10.1016/j.jclepro.2016.06.024.

[55] M. Eugenia Eugenio, D. Ibarra, R. Martín-Sampedro, E. Espinosa, I. Bascón, and A. Rodríguez, 'Alternative Raw Materials for Pulp and Paper Production in the Concept of a Lignocellulosic Biorefinery', in *Cellulose*, IntechOpen, 2019. doi: 10.5772/intechopen.90041.

[56] N. Sjöstedt, 'Isolation of cellulose fibres from agricultural waste Production of dissolving-grade pulp from oat husk and wheat straw'. [Online]. Available: www.chalmers.se

[57] P. Bajpai, 'Pulping Fundamentals', in *Biermann's Handbook of Pulp and Paper*, Elsevier, 2018, pp. 295–351.

[58] J.-C. Bonhivers and Paul. R. Stuart, 'Applications of Process Integration Methodologies in the Pulp and Paper Industry', in *Handbook of Process Integration (PI)*, Elsevier, 2013, pp. 765–798. doi: 10.1533/9780857097255.5.765.

[59] Y. Y. Tye, K. T. Lee, W. N. Wan Abdullah, and C. P. Leh, 'The world availability of non-wood lignocellulosic biomass for the production of cellulosic ethanol

and potential pretreatments for the enhancement of enzymatic saccharification', *Renewable and Sustainable Energy Reviews*, vol. 60, pp. 155–172, Jul. 2016, doi: 10.1016/j.rser.2016.01.072.

[60] S. Alila, I. Besbes, M. R. Vilar, P. Mutjé, and S. Boufi, 'Non-woody plants as raw materials for production of microfibrillated cellulose (MFC): A comparative study', *Ind Crops Prod*, vol. 41, pp. 250–259, Jan. 2013, doi: 10.1016/j.indcrop.2012.04.028.

[61] S. J. Owonubi, S. C. Agwuncha, N. M. Malima, G. B. Shombe, E. M. Makhatha, and N. Revaprasadu, 'Non-woody Biomass as Sources of Nanocellulose Particles: A Review of Extraction Procedures', *Front Energy Res*, vol. 9, Apr. 2021, doi: 10.3389/fenrg.2021.608825.

[62] M. A. Azeez, 'Pulping of Non-Woody Biomass', in *Pulp and Paper Processing*, InTech, 2018. doi: 10.5772/intechopen.79749.

[63] D. M. Le, H. R. Sørensen, N. O. Knudsen, and A. S. Meyer, 'Implications of silica on biorefineries – interactions with organic material and mineral elements in grasses', *Biofuels, Bioproducts and Biorefining*, vol. 9, no. 1, pp. 109–121, Jan. 2015, doi: 10.1002/bbb.1511.

[64] J. C. Solarte-Toro, J. A. Arrieta-Escobar, B. Marche, and C. A. Cardona Alzate, 'Effect of the lignin extraction process on the economics of a woody-based biorefinery', 2021, pp. 1871–1876. doi: 10.1016/B978-0-323-88506-5.50290-4.

[65] M. Sharma, A. Simões, P. Alves, and L. M. Gando- Ferreira, 'Efficient Recovery of Lignin and Hemicelluloses from Kraft Black Liquor', *KnE Materials Science*, Aug. 2022, doi: 10.18502/kms.v7i1.11602.

[66] L. Kouisni, P. Holt-Hindle, K. Maki, and M. Paleologou, 'The LIGNOFORCE SYSTEM™: A new process for the production of high-quality lignin from black liquor', 2012.

[67] M. A. Hubbe, R. Alén, M. Paleologou, M. Kannangara, and J. Kihlman, 'Lignin recovery from spent alkaline pulping liquors using acidification, membrane separation, and related processing steps: A Review', *Bioresources*, vol. 14, no. 1, pp. 2300–2351, 2019, doi: 10.15376/biores.14.1.Hubbe.

[68] R. Sun, J. Tomkinson, and J. Bolton, 'Effects of precipitation pH on the physico-chemical properties of the lignins isolated from the black liquor of oil palm empty fruit bunch fibre pulping', *Polym Degrad Stab*, vol. 63, no. 2, pp. 195–200, Feb. 1999, doi: 10.1016/S0141-3910(98)00091-3.

[69] S. Jose, L. Mishra, G. Basu, and A. Kumarsamanta, 'Study on Reuse of Coconut Fiber Chemical Retting Bath. Part II---Recovery and Characterization of Lignin', *Journal of Natural Fibers*, pp. 1–9, Apr. 2017, doi: 10.1080/15440478.2016.1212772.

[70] J. M. Carbajo and F. Maraver, 'Sulphurous Mineral Waters: New Applications for Health', *Evidence-Based Complementary and Alternative Medicine*, vol. 2017, pp. 1–11, 2017, doi: 10.1155/2017/8034084.

[71] F. Products and C. Engineering, ‘Thesis for the degree of Licentiate of Engineering: Dusting in a lime kiln, Characterization of the material and unit operations, Henric Dernegård’.

[72] V. Ribeiro dos Santos, M. Dezena Cabrelon, E. de Sousa Trichês, and E. Quinteiro, ‘Green liquor dregs and slaker grits residues characterization of a pulp and paper mill for future application on ceramic products’, *J Clean Prod*, vol. 240, p. 118220, Dec. 2019, doi: 10.1016/j.jclepro.2019.118220.

[73] Maria. Mäkitalo and Luleå tekniska universitet. Institutionen för samhällsbyggnad och naturresurser., *Green liquor dregs as sealing layer material to cover sulphidic mine waste deposits*. Luleå tekniska universitet, 2012.

[74] M. Mäkitalo, C. Maurice, Y. Jia, and B. Öhlander, ‘Characterization of Green Liquor Dregs, Potentially Useful for Prevention of the Formation of Acid Rock Drainage’, *Minerals*, vol. 4, no. 2, pp. 330–344, Apr. 2014, doi: 10.3390/min4020330.

[75] ‘User Guidelines for Waste and Byproduct Materials in Pavement Construction’. Accessed: Oct. 20, 2023. [Online]. Available: https://www.fhwa.dot.gov/publications/research/infrastructure/structures/97148/ssa1.cfm#:~:text=Steel%20slag%2C%20a%20by%2Dproduct,oxides%20that%20solidifies%20upon%20cooling.

[76] ‘Sequestration of carbon dioxide in steel slag, Sushanth Kombathula, KTH Royal Institute of Technology, School of Industrial Engineering and Management’.

[77] M. Bodor, R. Santos, T. Gerven, and M. Vlad, ‘Recent developments and perspectives on the treatment of industrial wastes by mineral carbonation — a review’, *Open Engineering*, vol. 3, no. 4, Jan. 2013, doi: 10.2478/s13531-013-0115-8.

[78] M. Tu *et al.*, ‘Aqueous Carbonation of Steel Slag: A Kinetics Study’, *ISIJ International*, vol. 55, no. 11, pp. 2509–2514, 2015, doi: 10.2355/isijinternational.ISIJINT-2015-142.

[79] J. Behin and M. Zeyghami, ‘Dissolving pulp from corn stalk residue and waste water of Merox unit’, *Chemical Engineering Journal*, vol. 152, no. 1, pp. 26–35, Oct. 2009, doi: 10.1016/j.cej.2009.03.024.

[80] C. Heitner, D. Dimmel, and J. Schmidt, Eds., *Lignin and Lignans*. CRC Press, 2016. doi: 10.1201/EBK1574444865.

[81] I. K. Stoll, N. Boukis, and J. Sauer, ‘Syngas Fermentation to Alcohols: Reactor Technology and Application Perspective’, *Chemie Ingenieur Technik*, vol. 92, no. 1–2, pp. 125–136, Jan. 2020, doi: 10.1002/cite.201900118.

[82] C. I. Harding and E. R. Hendrickson, ‘Foam Fractionation of Black Liquor From Sulfate Pulping’, *J Air Pollut Control Assoc*, vol. 14, no. 12, pp. 491–499, Dec. 1964, doi: 10.1080/00022470.1964.10468321.

[83] V. R. Coterio, G. H. Luttrell, G. T. Adel, and M. Mankosa, 'Optimization of air-injection spargers for column flotation applications', 2016.

[84] A. K. Patel and B. N. Thorat, 'Gamma ray tomography—An experimental analysis of fractional gas hold-up in bubble columns', *Chemical Engineering Journal*, vol. 137, no. 2, pp. 376–385, Apr. 2008, doi: 10.1016/j.cej.2007.05.014.

[85] M. Elia, T. McDonald, and A. Crisp, 'Errors in measurements of CO_2 with the use of drying agents', *Clinica Chimica Acta*, vol. 158, no. 3, pp. 237–244, Aug. 1986, doi: 10.1016/0009-8981(86)90287-1.

[86] Z. Koshraftar, A. Ghaemi, and H. Mashhadimoslem, 'Evaluation of the Silica Gel Adsorbent Potential for Carbon Dioxide Capture: Experimental and Modeling', *Iranian Journal of Chemical Engineering*, vol. 18, no. 4, pp. 64–80, 2021, doi: 10.22034/ijche.2022.335792.1425.

[87] Y. Xia, S. Moran, E. P. Nikonowicz, and X. Gao, 'Z-restored spin-echo ^{13}C 1D spectrum of straight baseline free of hump, dip and roll', *Magnetic Resonance in Chemistry*, vol. 46, no. 5, pp. 432–435, May 2008, doi: 10.1002/mrc.2195.

[88] G. Besagni, F. Inzoli, and T. Ziegenhein, 'Two-Phase Bubble Columns: A Comprehensive Review', *ChemEngineering*, vol. 2, no. 2, p. 13, Mar. 2018, doi: 10.3390/chemengineering2020013.

[89] '11 Bubble Column Reactors', 2002, pp. 327–366. doi: 10.1016/S1874-5970(02)80012-1.

[90] F. Milella and M. Mazzotti, 'Estimating speciation of aqueous ammonia solutions of ammonium bicarbonate: application of least squares methods to infrared spectra', *React Chem Eng*, vol. 4, no. 7, pp. 1284–1302, 2019, doi: 10.1039/C9RE00137A.

[91] U. Lichtfers and B. Rumpf, 'Infrarotspektroskopische Untersuchungen zur Ermittlung von Spezieskonzentrationen in wässrigen Lösungen, die Ammoniak und Kohlendioxid enthalten', *Chem Ing Tech*, vol. 72, no. 12, pp. 1526–1530, 2000, doi: 10.1002/1522-2640(200012)72:12<1526::AID-CITE1526>3.0.CO;2-8.

[92] M. Yoo, S.-J. Han, and J.-H. Wee, 'Carbon dioxide capture capacity of sodium hydroxide aqueous solution', *J Environ Manage*, vol. 114, pp. 512–519, Jan. 2013, doi: 10.1016/j.jenvman.2012.10.061.

[93] N. H. Do *et al.*, 'The novel method to reduce the silica content in lignin recovered from black liquor originating from rice straw', *Sci Rep*, vol. 10, no. 1, p. 21263, Dec. 2020, doi: 10.1038/s41598-020-77867-5.

[94] J. V. G. Tinio, K. T. Simfroso, A. D. M. V. Peguit, and R. T. Candidato, 'Influence of OH^- Ion Concentration on the Surface Morphology of ZnO-SiO_2 Nanostructure', *J Nanotechnol*, vol. 2015, pp. 1–7, 2015, doi: 10.1155/2015/686021.

[95] Y. Liu *et al.*, 'A sustainable route for the preparation of activated carbon and silica from rice husk ash', *J Hazard Mater*, vol. 186, no. 2–3, pp. 1314–1319, Feb. 2011, doi: 10.1016/j.jhazmat.2010.12.007.

[96] P. Lu and Y.-L. Hsieh, 'Highly pure amorphous silica nano-disks from rice straw', *Powder Technol*, vol. 225, pp. 149–155, Jul. 2012, doi: 10.1016/j.powtec.2012.04.002.

[97] 'SpectraBase, (n.d.). Sodium carbonate', John Wiley & Sons, Inc.

[98] F. M. Baena-Moreno, M. Rodríguez-Galán, F. Vega, T. R. Reina, L. F. Vilches, and B. Navarrete, 'Synergizing carbon capture storage and utilization in a biogas upgrading lab-scale plant based on calcium chloride: Influence of precipitation parameters', *Science of The Total Environment*, vol. 670, pp. 59–66, Jun. 2019, doi: 10.1016/j.scitotenv.2019.03.204.

[99] Y. Jia, R. Hamberg, A. Qureshi, M. Mäkitalo, and C. Maurice, 'Variation of green liquor dregs from different pulp and paper mills for use in mine waste remediation', *Environmental Science and Pollution Research*, vol. 26, no. 30, pp. 31284–31300, Oct. 2019, doi: 10.1007/s11356-019-06180-0.

[100] A. I. de Oliveira *et al.*, 'Use of Dregs as a Replacement for Hydrated Lime in Cement Coating Mortar', *Journal of Composites Science*, vol. 7, no. 5, p. 181, May 2023, doi: 10.3390/jcs7050181.

[101] R. V. Eleutério, L. Simão, P. Lemes, and D. Hotza, 'Evaluation of As-Received Green Liquor Dregs and Biomass Ash Residues from a Pulp and Paper Industry as Raw Materials for Geopolymers', *Minerals*, vol. 13, no. 9, p. 1158, Aug. 2023, doi: 10.3390/min13091158.

[102] A. Z. Johannes and R. K. Pingak, 'A comprehensive XRD analysis of $CaCO_3$ from Tablolong Beach sand as a potential smart material resource', in *American Institute of Physics Conference Series*, 2021, p. 020018. doi: 10.1063/5.0062186.

[103] T. THRIVENI, J. Whan AHN, and C. RAMAKRISNA, 'Arsenic Oxyanions Removal from Waste Water by Accelerated Carbonation', *Journal of MMIJ*, vol. 133, no. 1, pp. 1–3, 2017, doi: 10.2473/journalofmmij.133.1.

[104] R. Ševčík, P. Šašek, and A. Viani, 'Physical and nanomechanical properties of the synthetic anhydrous crystalline $CaCO_3$ polymorphs: vaterite, aragonite and calcite', *J Mater Sci*, vol. 53, no. 6, pp. 4022–4033, Mar. 2018, doi: 10.1007/s10853-017-1884-x.

[105] B. Sun, H. Zhou, M. Arowo, J. Chen, J. Chen, and L. Shao, 'Preparation of basic magnesium carbonate by simultaneous absorption of NH_3 and CO_2 into $MgCl_2$ solution in an RPB', *Powder Technol*, vol. 284, pp. 57–62, Nov. 2015, doi: 10.1016/j.powtec.2015.06.043.